Theoretical study on the photodissociation process of ICl molecule

March 2014

Takahide Matsuoka

主　論　文　要　旨

報告番号	㊙　乙　第　　号	氏　名	松岡　貴英

主 論 文 題 目 :

Theoretical study on the photodissociation process of ICl molecule

(ICl 分子の光解離過程に関する理論的研究)

（内容の要旨）

量子論的効果が顕著な系にあって，その化学反応を定量的に予測することはいまでも困難である．特に，非断熱相互作用が重要になるとき，量子効果がその結果に顕著に現われる．筆者は，低励起状態において多くの非断熱相互作用の存在が分かっている ICl 分子に焦点を当て，その光解離過程において量子論的効果が及ぼす影響の詳細を理論的に解析した．

第一章では，非断熱相互作用に関する基礎事項とそれが光解離過程に及ぼす影響ついて説明した．また，非断熱遷移の理論計算の現状および問題をまとめ，本論文の目的と背景を述べた．

第二章では，ICl 分子の低励起状態，遷移双極子モーメントの計算に用いた線形応答理論，光解離生成物の角運動量分極が内包する量子論的情報，非断熱遷移の半古典論的取り扱い，のそれぞれについて説明した．

第三章では，遷移双極子モーメントの定量性を検討するため，ICl 分子よりもスピン軌道相互作用の弱い Cl_2 分子について，電子相関を異なるレベルで取り入れた計算方法を用いて length-form の遷移双極子モーメントと線形応答理論による遷移双極子モーメントの比較と検討を行った．遷移双極子モーメントが，計算に用いる一電子軌道に顕著に依存することを明らかにした．また，length-form の遷移双極子モーメントの有効性について述べた．

第四章では，ICl 分子の第１吸収帯の光解離過程について議論した．解離生成物の角運動量分極，解離方向異方性，生成物分岐比を，波束伝搬法を用いて計算し，実験結果との比較検討を行った．短波長領域においては 1(II)状態への光励起が支配的になるため，解離方向の異方性には垂直成分が強くなることを明らかにした．X(0^+)状態と 0^+(II)状態間の非断熱遷移が，顕わな回避交差を持たない状態間の非断熱遷移であることを明らかにした．非断熱遷移確率を計算するためにはポテンシャルエネルギーの情報だけでは不十分であることを指摘した．

第五章では，ICl 分子の第２吸収帯の光解離過程について議論した．解離方向異方性と生成物分岐比について，波束伝搬法，半古典論, 古典軌跡法の３種類の方法で計算し，実験結果との比較検討を行った．0^+(III)状態と 0^+(IV)状態の間の量子干渉効果によって， I+Cl チャネルの平行成分が弱められることを明らかにした．基底状態 X(0^+)からの２電子励起配置を主配置とする 0^+(IV)状態が，0^+(III)状態と同程度の光吸収強度を持つ機構について議論した．以上を踏まえて，同程度の吸収強度と励起エネルギーを持つ状態間で非断熱遷移が起きる場合において量子干渉効果が無視できないことを明らかにし，量子干渉効果を計算するためには電子状態の位相の情報を保持することの重要性について指摘した．ポテンシャルエネルギー曲線の形状から，この量子干渉効果の特徴を考察した．また，種々の動力学計算方法について，それぞれの問題点について議論した．

第六章では，本論文の統括を行い，量子干渉効果が影響しうる場合について議論した．

SUMMARY OF Ph.D. DISSERTATION

School	Student Identification Number	SURNAME, First name
School of Fundamental Science and Technology		MATSUOKA, Takahide

Title

Theoretical study on the photodissociation process of ICl molecule

Abstract

Quantitative prediction of chemical reactions is still difficult task in systems with considerable quantum effect. Specifically, if the non-adiabatic interaction is significant, the quantum effect may have a large impact on the results. The author focused on ICl molecule, in which numerous non-adiabatic transitions among the low-lying excited states exist, and analyzed theoretically the quantum effects in its photodissociation process in detail.

In Chapter 1, the fundamentals of non-adiabatic interactions and their effects on photodissociation process were described. The current status and the issues of the non-adiabatic transition theory were summarized, and the purpose of this thesis was clarified.

In Chapter 2, the low-lying excited states of ICl, the linear response theory applied to the calculations of transition dipole moments, the quantum information included in the photofragment angular momentum polarization, and the semi-classical treatment of non-adiabatic transitions were reviewed.

In Chapter 3, for the purpose of the accuracy assessment for transition dipole moments, those of Cl_2, whose spin-orbit effect is weaker than those of ICl, were examined in the length-form and in the linear response treatment, including the electronic correlations at various different levels. A significant dependence of the transition dipole moments on the one-electron orbitals used in the calculation was clarified. The validity of the length-form was also discussed.

In Chapter 4, the photodissociation process of ICl in the first absorption band was discussed. The photofragment angular momentum polarization, the anisotropy parameters, and the product branching ratios were calculated with the wave packet propagation method, and were examined in comparison with the experiments. The strong perpendicular component of the product angular distribution in the shorter wavelength region was attributed to the dominating photoexcitation to the 1(II) state. The non-adiabatic transition between the $X(0^+)$ and 0^+(II) states was found to be of Landau-Zener type without explicit avoided crossing, implying the information of the potential energies alone is insufficient for calculating the non-adiabatic transition probabilities.

In Chapter 5, the photodissociation process of ICl in the second absorption band was discussed. The anisotropy parameters and the product branching ratios were calculated with three methods, namely, the wave packet propagation method, the semi-classical method, and the classical path method, and were examined in comparison with recent experiments. The parallel component of the I+Cl channel products was significantly reduced by the destructive interference effect between the 0^+(III, IV) states. The mechanism for the 0^+(IV) state, which is dominated by the doubly excited configuration from the $X(0^+)$ state, to have a comparable transition dipole moment magnitude with the 0^+(III) state was discussed. Based upon the results, the author clarified that the interference effect must always be considered whenever the relevant states have comparable excitation energies and photoabsorption intensities, and exhibit non-adiabatic transition. He also indicated the importance of conserving the phase information of the electronic state in the assessment of interference effect. The characteristics of the interference effect were examined from the potential energy curves of the 0^+(III,IV) states. The issues of the various calculation methods of dynamics were discussed.

In Chapter 6, the author summarized the results and discussed the cases in which the quantum interference can be effective.

A Thesis for the Degree of Ph.D. in Science

Theoretical study on the photodissociation process of ICl molecule

March 2014

Graduate School of Science and Technology

Keio University

Takahide Matsuoka

Acknowledgements

First and foremost, I would like to extend my utmost gratitude to my supervisor Prof. Dr. Satoshi Yabushita at Keio University for the continuous support throughout the course of this thesis. I thank him for his in-depth guidance and patience. His endless efforts to train me as a researcher has been my driving force to deliver this thesis. His advice on both research as well as on my career have been priceless.

I would like to also thank Prof. Dr. Mikio Eto, Prof. Dr. Naoki Yoshioka, and Prof. Dr. Hiroshi Kondoh for their kind advices on completing this thesis and illuminating discussions about the research.

I am greatly indebt to Dr. Michihiko Sugawara for his detailed advice on completing the essential program used in this research and for insightful and concrete discussions on the theoretical approaches for dynamics. I have also enjoyed sharing the experiences in computations for official research and for casual programming.

Finally, I would like to thank my parents for giving me the opportunity to deliver this thesis. It has provided countless precious experiences within my life and flooding good memories at the laboratory. Thank you.

Contents

Chapter 1
General Introduction

In this chapter, the author explains the scope and the subject of this thesis. Firstly, the importance of the non-adiabatic transition theory is explained in 1.1. Then the fundamentals of non-adiabatic interactions and their effects on photodissociation process are described in 1.2. Lastly, the concrete subject of this thesis is defined in 1.3.

1.1 Quantum effects in chemical reaction

The Born-Oppenheimer approximation [1] relies on the fact that the rest mass even of the lightest proton m_{p} is significantly heavier than that of electron $m_{\mathrm{p}}/m_{\mathrm{e}} \approx 1836$, and the motion of electrons could follow the slower movement of nuclei. This approximation has been proven to be satisfied in predicting a chemical reaction within the region, where the adiabatic electronic state is not degenerate with other states. However, in chemical reactions of large systems or in highly excited electronic states, this approximation is likely to break down and the non-adiabatic interaction must be considered. The author would like to quote Felix T. Smith [2],

"*I believe that calculations based on a single-potential energy surface will be of very limited usefulness in the real world of chemically reacting systems, and that electronic transitions between a multiplicity of states are likely to play a very large role in such events. Even where adiabatic calculations with a single potential surface are valid, it is desirable to demonstrate their validity, and this can only be done in the framework of a theory which takes proper account of all the couplings between states that may exist, so that they can be evaluated and proved to be small. If these coupling are strong, quantum effects associated with such nonadiabatic behavior may prove to be one of the most important features of many chemical reaction processes. Probably such quantum effects will turn out to be more important than the quantum effects associated with barrier leakage and vibrational zero point energy that are often discussed in connection with the movement of systems over adiabatic surfaces.*"

Although properties of single adiabatic electronic state can often be chemically interpreted with the help of theoretical quantum chemistry, quantum effect in the chemical process may make it difficult to describe the state in a single electronic state. The rapid development and application to large systems of computational chemistry has led to an urgent need for the establishment of the methodology for the treatment of quantum effect.

In this dissertation, the author focused on the photodissociation process of ICl molecule, in which numerous non-adiabatic transitions among the low-lying excited

states exist, and analyzed theoretically the quantum effects in its photodissociation process.

1.2 Photodissociation process of diatomic molecules

1.2.1 External field as an perturbation

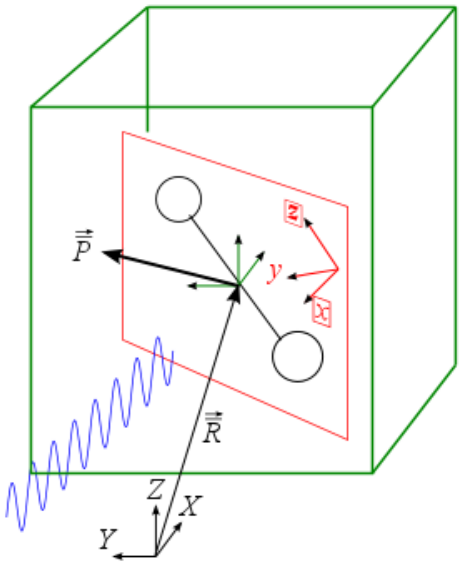

Figure 1-1: Figure describing the laboratory frame (black), the center-of-mass frame (green), and the molecular frame (red).

In order to explicitly describe how the photodissociation process is treated, this section explains the theoretical framework, which has been applied to the calculation in this thesis. We consider two eigenstates Ψ_I and Ψ_F of the time-independent Hamiltonian $\hat{H}^{(0)}$ of the center-of-mass frame molecular system, with the center-of-mass position vector defined with respect to the origin of the laboratory frame as $\vec{R}$. Neglecting the effect of the center-of-mass momentum, $\vec{P}$, in the center-of-mass frame system, the two

wave functions in the laboratory frame can be written as, $h^{-3/2}e^{i\vec{\vec{P}}_I\cdot\vec{\vec{R}}/\hbar}\Psi_I$ and $h^{-3/2}e^{i\vec{\vec{P}}_F\cdot\vec{\vec{R}}/\hbar}\Psi_F$, where h denotes Planck's constant with the normalization factor of the plane waves describing the translational motion being $h^{-3/2}$ [3], and Ψ_I and Ψ_F denote the wave functions of the internal degrees of freedom in the center-of-mass frame at $t = 0$, $\Psi_I(t = 0)$, $\Psi_F(t = 0)$, respectively. With the laboratory frame time-dependent perturbation $\hat{H}^{(1)}(t)$ treated as a first-order perturbation to the initial wave function in the state I with the translational momentum $\vec{\vec{P}}_I$, $h^{-3/2}e^{i\vec{\vec{P}}_I\cdot\vec{\vec{R}}/\hbar}\Psi_I$, the amplitude $a_{FI}(t)$ of the wave function in the final state $h^{-3/2}e^{i\vec{\vec{P}}_F\cdot\vec{\vec{R}}/\hbar}\Psi_F(t)$ is given as, $a_{FI}(t,\vec{\vec{P}}_I,\vec{\vec{P}}_F) = -\frac{2\pi i}{h^4}\int_0^t\int\left\langle e^{i\vec{\vec{P}}_F\cdot\vec{\vec{R}}/\hbar}\Psi_F(t')\middle|\hat{H}^{(1)}(t')\middle|e^{i\vec{\vec{P}}_I\cdot\vec{\vec{R}}/\hbar}\Psi_I(t')\right\rangle d\vec{\vec{R}}dt'$. In the classical electrodynamics, if the plane polarized light with wavelength λ, propagating along the laboratory X axis in the vacuum with the field vector in the $+Z$ direction, $\vec{E}(t) = \vec{e}_Z E_0\sin(2\pi X/\lambda - \omega t))$, is treated as the time-dependent perturbation to the laboratory frame molecular system, the transition amplitude with the application of the dipole approximation is given as follows,

$$\begin{aligned} a_{FI}(t,\vec{\vec{P}}_I,\vec{\vec{P}}_F) &= -\frac{2\pi i E_0}{h^4}\int_0^t\left\langle\Psi_F(t')\middle|\hat{\mu}_Z\middle|\Psi_I(t')\right\rangle\int e^{-i\vec{\vec{P}}_F\cdot\vec{\vec{R}}/\hbar}\sin(2\pi\overline{X}/\lambda - \omega t')e^{i\vec{\vec{P}}_I\cdot\vec{\vec{R}}/\hbar}d\vec{\vec{R}}dt' \\ &= -\frac{E_0}{2\hbar}\int_0^t\left\langle\Psi_F(t')\middle|\hat{\mu}_Z\middle|\Psi_I(t')\right\rangle\left[e^{-i\omega t'}\delta(\vec{\vec{P}}_F - \vec{\vec{P}}_I - h\vec{e}_X/\lambda) - e^{i\omega t'}\delta(\vec{\vec{P}}_F - \vec{\vec{P}}_I + h\vec{e}_X/\lambda)\right]dt'. \end{aligned} \quad (1\text{-}1)$$

Here, $\hat{\mu}_Z$ denotes the Z-component of the dipole operator. The first term in the square brackets is for the case the associated translational momentum is increased by $h\vec{e}_X/\lambda$, then $\vec{\vec{P}}_F = \vec{\vec{P}}_I + h\vec{e}_X/\lambda$, hence corresponds to the light absorption of the molecule. On the contrary, the second term is for the case the momentum is decreased by $h\vec{e}_X/\lambda$,

then $\vec{\vec{P}}_F = \vec{\vec{P}}_I - h\vec{e}_X/\lambda$, hence corresponds to the light emission of the molecule. Therefore, the transition amplitude for the light absorption and the total photoabsorption cross-section is given as,

$$a_{FI}(t) = -\frac{E_0}{2\hbar}\left\langle \Psi_F \left| \hat{\mu}_Z \right| \Psi_I \right\rangle \int_0^t \exp\left[\frac{\mathrm{i}}{\hbar}(E_F - E_I - \hbar\omega)t'\right]\mathrm{d}t', \tag{1-2}$$

$$\sigma^{\mathrm{abs}}(\omega) = \frac{\omega}{\hbar\varepsilon_0 c}\mathrm{Re}\left[\left\langle \Psi_I \left| \hat{\mu}_Z \right| \Psi_F \right\rangle \cdot \int_0^\infty \exp\left(\frac{\mathrm{i}}{\hbar}(\hbar\omega + E_I - E_F)t\right)\mathrm{d}t \cdot \left\langle \Psi_F \left| \hat{\mu}_Z \right| \Psi_I \right\rangle\right]. \tag{1-3}$$

Here, ε_0 and c denote the vacuum permittivity and the speed of light, respectively. Strictly, E_F and E_I are the energies of the final and initial states, respectively, hence their energy difference includes the one due to the change of the translational kinetic energy. The contribution of the translational momentum causes the broadening of the cross-section, namely the Doppler broadening [4]. Here, the translational momentum is considered to be narrowly-distributed and the Doppler effect on the parent molecule is neglected. Therefore, E_F and E_I are taken as the eigenvalues of the Ψ_F and Ψ_I, respectively. Applying the Born-Oppenheimer approximation, which hitherto was not considered, the total wave function Ψ_F is expanded in terms of nuclear wave function $\chi_{F,n}(\vec{R})$ for relative motions, which includes the phases of the matter waves, with adiabatic electronic states $\psi_n(\vec{r};\vec{R})$ as, $\left|\Psi_F\right\rangle = \sum_n \left|\chi_{F,n}(\vec{R})\psi_n(\vec{r};\vec{R})\right\rangle$. Here, $\vec{r}$ and $\vec{R}$ denote the set of position vectors of electrons and the relative position vectors of the nuclei, respectively. If the initial state is in the ground adiabatic state X, $\left|\Psi_I\right\rangle = \left|\chi_I\psi_{\mathrm{X}}\right\rangle$, and the electronic photoexcitation is considered, $\left\langle \chi_{F,\tilde{n}}\psi_{\tilde{n}} \left| \hat{\mu}_Z \right| \Psi_I \right\rangle = \left\langle \chi_{F,\tilde{n}} \left| \mu_{Z,\tilde{n}\mathrm{X}} \right| \chi_I \right\rangle$,

where $\mu_{Z,\tilde{n}\mathrm{X}}$ denotes the *Z*-component of the electronic transition dipole moment from the ground adiabatic state X to the excited adiabatic state $\tilde{n}$, which is the Franck-Condon electronic state, namely, the electronic state in the molecular region, the absorption cross-section for the photodissociation process is given as [5],

$$\sigma^{\mathrm{abs}}(\omega) = \frac{\omega}{\hbar\varepsilon_0 c}\sum_{\tilde{n}} \mathrm{Re}\left[\int_0^\infty \left\langle \chi_I \left| \mu_{Z,\mathrm{X}\tilde{n}} \exp\left(\frac{i}{\hbar}(E_I + \hbar\omega - E_F)t\right)\right| \chi_{F,\tilde{n}}\right\rangle \left\langle \chi_{F,\tilde{n}} \left| \mu_{Z,\tilde{n}\mathrm{X}} \right| \chi_I \right\rangle \mathrm{d}t\right] \quad (1\text{-}4$$

$$= \frac{\omega}{\hbar\varepsilon_0 c}\sum_{\tilde{n}} \mathrm{Re}\left[\int_0^\infty \exp(\mathrm{i}Et/\hbar)\left\langle \xi_{\tilde{n}} \left| \xi_{\tilde{n}}(t)\right\rangle \mathrm{d}t\right]. \quad)$$

E denotes the sum of the initial energy and the photoexcitation energy, $E = E_I + \hbar\omega$, and $\xi_{\tilde{n}}$ denotes the initial Franck-Condon wave packet of the excited adiabatic state $\tilde{n}$, $\left|\xi_{\tilde{n}}\right\rangle = \left|\psi_{\tilde{n}}\right\rangle \mu_{Z,\tilde{n}\mathrm{X}} \left|\chi_I\right\rangle$, which propagates in time t as $\left|\xi_{\tilde{n}}(t)\right\rangle = \mathrm{e}^{-i\hat{H}^{(0)}t/\hbar}\left|\xi_{\tilde{n}}\right\rangle$. It should be noted that if the Hamiltonian $\hat{H}^{(0)}$ includes the non-adiabatic interaction, the Franck-Condon wave packet can be expressed as superposition of multiple adiabatic electronic states, $\left|\xi_{\tilde{n}}(t)\right\rangle = \sum_n a_{\tilde{n},n}(t)\left|\psi_n\right\rangle$, and $\tilde{n}$ only denotes the initial electronic state.

If the parent molecule is considered to be randomly oriented with its total angular momentum quantum number being J_I, the cross-section for the parent molecule is averaged over the states with those component quantum number M_I. In this way, the photoproduct differential cross-section can be expressed in terms of the scattering T matrix elements $\left\langle \Psi_F^{-(\vec{k})} \left| \hat{\mu}_Z \right| \Psi_{I,J_I,M_I} \right\rangle$, with $\vec{k}$ being the recoil vector of the photofragments, and the anisotropy parameter β, as follows [5–7],

$$\sigma(\vec{k},\omega) = \frac{\pi\omega}{\varepsilon_0 c(2J_I+1)} \sum_{M_I} \left| \left\langle \Psi_F^{-(\vec{k})} \left| \hat{\mu}_Z \right| \Psi_{I,J_I,M_I} \right\rangle \right|^2$$
$$= \frac{\pi\omega}{\varepsilon_0 c(2J_I+1)} \sum_{M_I,n} \left| \sum_{\tilde{n}} \left\langle \chi_{F,\tilde{n},n}^{-(\vec{k})} \left| \mu_{Z,\tilde{n}\mathrm{X}} \right| \chi_{I,J_I,M_I} \right\rangle \right|^2 \qquad (1\text{-}5)$$
$$\propto 1 + \beta P_2(\cos\theta).$$

Here, $P_2(\cos\theta)$ is the Legendre polynomial for $\cos\theta$, $P_2(\cos\theta) = (3\cos^2\theta - 1)/2$, where θ is the angle between the recoil vector $\vec{k}$ and the field vector $\vec{e}_Z$. In a classical treatment, the angle between the initial molecular axis and the recoiling vector, γ, can be evaluated by the half-collision trajectory calculation on a single potential, $V(R)$, from the classical turning point, R_T, to the dissociation limit, as follows [4,8],

$$\gamma = \sqrt{\frac{\hbar^2 J_I^2}{2\mu}} \int_{R_\mathrm{T}}^{\infty} \left[V(R_\mathrm{T}) - V(R) + \frac{\hbar^2 J_I^2}{2\mu} \left(\frac{1}{R_\mathrm{T}^2} - \frac{1}{R^2} \right) \right]^{-1/2} \frac{\mathrm{d}R}{R^2}. \qquad (1\text{-}6)$$

μ denotes the reduced mass of the diatomic molecule. If the rotational motion of the parent diatomic molecule is not highly excited, the linear momentum in the rotating direction $\hbar J_I / R_\mathrm{e}$, where R_e is the equilibrium internuclear distance, is negligible compared to the recoiling momentum $\hbar|\vec{k}|$, $\hbar J_I / R_\mathrm{e} << \hbar|\vec{k}|$, the so-called axial recoil approximation, which considers the molecular axis of the parent molecule, $\vec{R}$, coincides with the recoil vector $\vec{k}$, $\gamma = 0$, is valid [4].

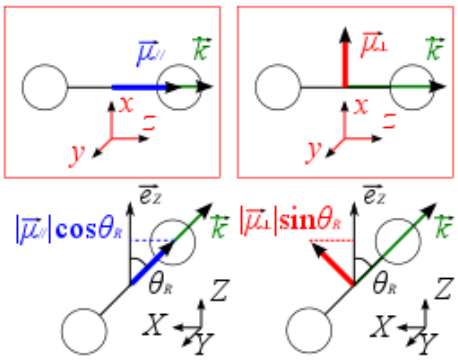

Figure 1-2: Figure indicating the transition dipole moment in molecular frame (red box) and laboratory frame.

Transforming the electronic dipole operator from the laboratory frame to the molecular frame, $\hat{\mu}_Z = \hat{\mu}_{//}\cos\theta_R + \hat{\mu}_{\perp}\sin\theta_R$, where θ_R being the angle between the molecular axis $\vec{R}$ and the field vector $\vec{e}_Z$ as shown in Figure 1-2, with the application of the axial recoil approximation, it is apparent from equation (1-5) that, if only the parallel transition is permitted, $\mu_{//,\tilde{n}X} \neq 0, \mu_{\perp,\tilde{n}X} = 0$, the corresponding differential cross section of the product is given as, $\sigma_{//}(\theta) \propto \left|\hat{\mu}_Z\right|^2 = \left|\hat{\mu}_{//}\right|^2 \cos^2\theta$, and the anisotropy parameter β equals 2, as shown in Figure 1-3 (a). On the other hand, if only the perpendicular transition is permitted, $\mu_{\perp,\tilde{n}X} \neq 0, \mu_{//,\tilde{n}X} = 0$, the differential cross section is given as, $\sigma_{\perp}(\theta) \propto \left|\hat{\mu}_Z\right|^2 = \left|\hat{\mu}_{\perp}\right|^2 \sin^2\theta$, and the anisotropy parameter β equals -1, as shown in Figure 1-3 (b). The respective selection rules for the parallel and perpendicular transition are $\Delta\Omega = 0$ and $\Delta\Omega = \pm 1$, where Ω is the molecular axis component of the total electronic angular momentum.

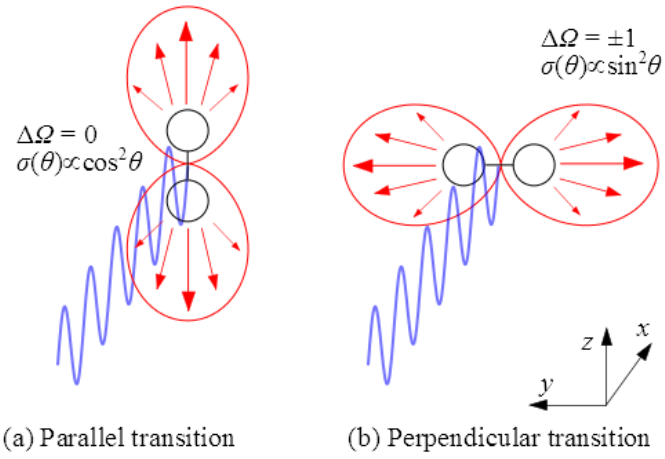

Figure 1-3: Schematic figure of photoproduct distribution for (a) a parallel transition and (b) a perpendicular transition of diatomic molecule.

The partial differential cross-sections of the channel n in the second line of equation (1-5) are given in the summation as,

$$\sigma_{n,n}(\vec{k},\omega) = \frac{\pi\omega}{\varepsilon_0 c(2J_I+1)} \sum_{M_I,n,\tilde{n}'} \left\langle \chi^{-(\vec{k})}_{F,\tilde{n},n} \middle| \mu_{Z,\tilde{n}X} \middle| \chi_{I,J_I,M_I} \right\rangle \left\langle \chi_{I,J_I,M_I} \middle| \mu_{Z,X\tilde{n}'} \middle| \chi^{-(\vec{k})}_{F,\tilde{n}',n} \right\rangle. \tag{1-7}$$

Although, in the absence of the non-adiabatic interaction, only the T matrix elements $\left\langle \chi^{-(\vec{k})}_{F,\tilde{n},n} \middle| \mu_{Z,\tilde{n}X} \middle| \chi_{I,J_I,M_I} \right\rangle$, whose electronic states in the Franck-Condon region and the dissociation limit are the same, $\tilde{n},\tilde{n}' = n$, would take non-zero value, the T matrix elements with $\tilde{n},\tilde{n}' \neq n$ must be taken into account if any non-adiabatic transitions may take place during the dissociating process. Hence, the T matrix element of the state n, $\left\langle \Psi^{-(\vec{k})}_{F,n} \middle| \hat{\mu}_Z \middle| \Psi_{I,J_I,M_I} \right\rangle$, is the superposition of the ones originating from all the Franck-Condon states $\tilde{n}$, and can be written as follows,

$$\left\langle \Psi^{-(\vec{k})}_{F,n} \middle| \hat{\mu}_Z \middle| \Psi_{I,J_I,M_I} \right\rangle = \sum_{\tilde{n}} \left\langle \chi^{-(\vec{k})}_{F,\tilde{n},n} \middle| \mu_{Z,\tilde{n}X} \middle| \chi_{I,J_I,M_I} \right\rangle. \tag{1-8}$$

In the dissociation limit, suppose Ω_A, Ω_B, Ω are the good quantum numbers for the electronic states of the two atoms, A and B, and the molecule, and the electronic state n correlates to the atomic angular momentum J_A and J_B, the molecular electronic state $\left|\psi_{n,\Omega}\right\rangle$ can then be expanded in terms of the electronic states of the two atoms as, $\left|\psi_{n,\Omega}\right\rangle = \sum_{\Omega_A} c_{n,\Omega,\Omega_A}\left|J_A,\Omega_A\right\rangle_A\left|J_B,\Omega-\Omega_A\right\rangle_B$, where c_{n,Ω,Ω_A} is the expansion coefficients. On the other hand, the tensor product of the electronic states of the two atoms in the dissociation limit is given as,

$$\left|J_A,\Omega_A\right\rangle_A\left|J_B,\Omega_B\right\rangle_B = \sum\nolimits_n c^*_{n,\Omega_A+\Omega_B,\Omega_A}\left|\psi_{n,\Omega_A+\Omega_B}\right\rangle. \tag{1-9}$$

The summation over the molecular state n is performed selectively from the group of states, correlating to the two atomic states in the lhs of equation (1-9), which are $(2J_A+1)\times(2J_B+1)$ in total. Similarly, the T matrix element for the corresponding atomic states is given as, $\left\langle \Psi^{-(\vec{k})}_{F;J_A,\Omega_A;J_B,\Omega_B}\left|\hat{\mu}_Z\right|\Psi_{I,J_I,M_I}\right\rangle = \sum_n c^*_{n,\Omega_A+\Omega_B,\Omega_A}\left\langle \Psi^{-(\vec{k})}_{F,n}\left|\hat{\mu}_Z\right|\Psi_{I,J_I,M_I}\right\rangle$. This T matrix element is considered as the coefficient of the two atoms dissociating with the momentum $\hbar\vec{k}$. Let the T matrix element be expressed in terms of its amplitude r_{Ω_A,Ω_B} and phase ϕ_{Ω_A,Ω_B}. The wave function of the two atoms in the dissociation limit is given as,

$$e^{i\vec{k}\cdot\vec{R}}\left|\psi_{J_A}\right\rangle_A\left|\psi_{J_B}\right\rangle_B = \sum\nolimits_{\Omega_A,\Omega_B} r_{\Omega_A,\Omega_B}\exp[i(\vec{k}\cdot\vec{R}+\phi_{\Omega_A,\Omega_B})]\left|J_A,\Omega_A\right\rangle_A\left|J_B,\Omega_B\right\rangle_B. \tag{1-10}$$

This expression elucidates the interpretation of the T matrix element as the amplitude r_{Ω_A,Ω_B} and phase ϕ_{Ω_A,Ω_B} of the matter wave for each of the corresponding atomic states $\left|J_A,\Omega_A\right\rangle_A\left|J_B,\Omega_B\right\rangle_B$. It should be noted that the sum of Ω_A and Ω_B is Ω, hence $\Omega_A + \Omega_B$ satisfies the selection rule of the light absorption transition, and especially when the

initial molecular electronic state is $\Omega_i=0^+$, r_{Ω_A,Ω_B} takes non-zero value only for $\Omega_A + \Omega_B=0$, ± 1 (Figure 1-4).

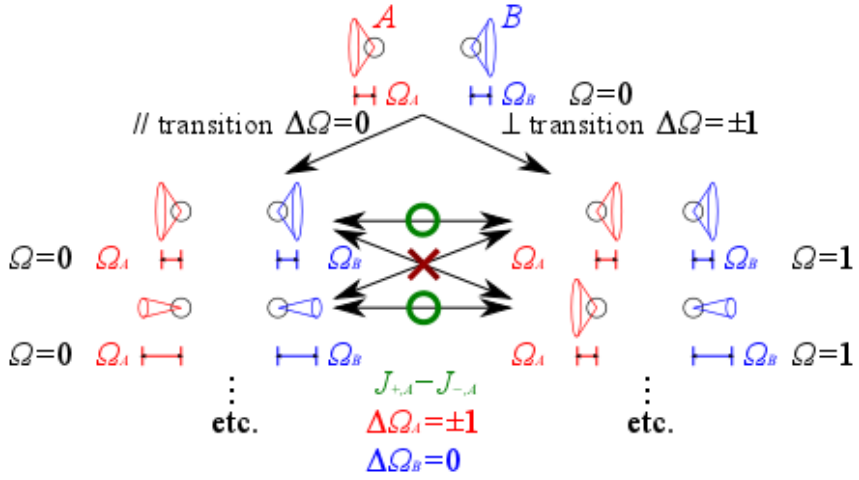

Figure 1-4: Schematic figure to explain the selection rule of the angular momenta.

Here, we define the molecular frame, whose z-axis is the recoil vector $\vec{k}$ and y-axis is perpendicular to plane containing the field vector $\vec{e}_Z$ (Z-axis in the laboratory frame) and the recoil vector $\vec{k}$. The expectation value of the y-component of the atom A's angular momentum $\hat{J}_{y,A}$, which can be expressed in terms of the raising and lowering operators $(\hat{J}_{+,A} - \hat{J}_{-,A})/2\mathrm{i}$, for the wave function in equation (1-10) is given as,

$$
\begin{aligned}
\left\langle \hat{J}_{y,A} \right\rangle &= {}_A\left\langle \psi_{J_A} \left| \frac{\hat{J}_{+,A} - \hat{J}_{-,A}}{2\mathrm{i}} \right| \psi_{J_A} \right\rangle_A \\
&= \sum_{\Omega_A,\Omega_B} \sqrt{J_A(J_A+1) - \Omega_A(\Omega_A+1)}\, r_{\Omega_A+1,\Omega_B} r_{\Omega_A,\Omega_B} \sin[\phi_{\Omega_A,\Omega_B} - \phi_{\Omega_A+1,\Omega_B}] \\
&= \sum_{\Omega_A} \sqrt{J_A(J_A+1) - \Omega_A(\Omega_A+1)}\, r_{\Omega_A+1,-\Omega_A} r_{\Omega_A,-\Omega_A} \sin[\phi_{\Omega_A,-\Omega_A} - \phi_{\Omega_A+1,-\Omega_A}] \\
&\quad - \sqrt{J_A(J_A+1) - \Omega_A(\Omega_A-1)}\, r_{\Omega_A-1,-\Omega_A} r_{\Omega_A,-\Omega_A} \sin[\phi_{\Omega_A,-\Omega_A} - \phi_{\Omega_A-1,-\Omega_A}] \qquad (1\text{-}11) \\
&\propto \frac{\sin\theta\cos\theta}{3}\sqrt{\frac{(1+\beta)(2-\beta)}{2}} \\
&\quad \times \sum_{\Omega_A} \sqrt{J_A(J_A+1) - \Omega_A(\Omega_A+1)}\, s_{\Omega_A+1,-\Omega_A} s_{\Omega_A,-\Omega_A} \sin[\phi_{\Omega_A,-\Omega_A} - \phi_{\Omega_A+1,-\Omega_A}] \\
&\quad - \sqrt{J_A(J_A+1) - \Omega_A(\Omega_A-1)}\, s_{\Omega_A-1,-\Omega_A} s_{\Omega_A,-\Omega_A} \sin[\phi_{\Omega_A,-\Omega_A} - \phi_{\Omega_A-1,-\Omega_A}].
\end{aligned}
$$

The summation over Ω_B is eliminated in the third line of equation (1-11) due to the selection rule of light absorption transition, $\Omega_A + \Omega_B = 0, \pm 1$. In the fourth line, the angle dependency of the amplitude r_{Ω_A,Ω_B}, which is the amplitude of the product recoiling with momentum $\hbar\vec{k}$, has been separated. The amplitudes of the parallel components $r_{\Omega_A,-\Omega_A}$ are the ones from the parallel transition $\mu_{//} \neq 0$, hence they are proportional to $\cos\theta$ and the angular dependence can be separated as, $r_{\Omega_A,-\Omega_A} \propto s_{\Omega_A,-\Omega_A}\cos\theta$. The angular dependence of the perpendicular components $r_{\Omega_A+1,-\Omega_A}$ are separated as, $r_{\Omega_A+1,-\Omega_A} \propto s_{\Omega_A+1,-\Omega_A}\sin\theta$. The newly introduced amplitudes $s_{\Omega_A,-\Omega_A}$ and $s_{\Omega_A+1,-\Omega_A}$ represent the square root of the probability fraction among the parallel and the perpendicular components, respectively, so that the sums of the probability densities of the parallel and perpendicular components equal to unity, $\sum_{\Omega_A}\left|s_{\Omega_A,-\Omega_A}\right|^2 = \sum_{\Omega_A}\left|s_{\Omega_A+1,-\Omega_A}\right|^2 = 1$.

It is apparent the expectation value $\left\langle \hat{J}_{y,A} \right\rangle$ maximizes its amplitude $\sqrt{(1+\beta)(2-\beta)}$ when β=0, namely, the intensity of the parallel and perpendicular transition is equal. This is due to the selection rule of the angular momentum operator $\hat{J}_{y,A}$ for the molecular state is $\Delta\Omega = \pm 1$, and the electronic state must be some mixed state consists of the parallel $\Omega = 0^+$ and the perpendicular $\Omega = 1$ components. Moreover, the presence of the phase difference of the parallel and the perpendicular components, $\phi_{\Omega_A,-\Omega_A} - \phi_{\Omega_A+1,-\Omega_A} = \phi_{\Omega=0+} - \phi_{\Omega=1}$ (note that $\Omega=\Omega_A+\Omega_B$), indicates that this observable is actually reflecting the quantum interference between the matter waves of the parallel and

the perpendicular components, which is the reminiscent of the Young's double slit experiment (Figure 1-5). The expectation value of the angular momentum $\langle \hat{J}_{y,A} \rangle$ is actually an expression of the first-rank angular momentum polarization parameter, which is further discussed in 2.3.

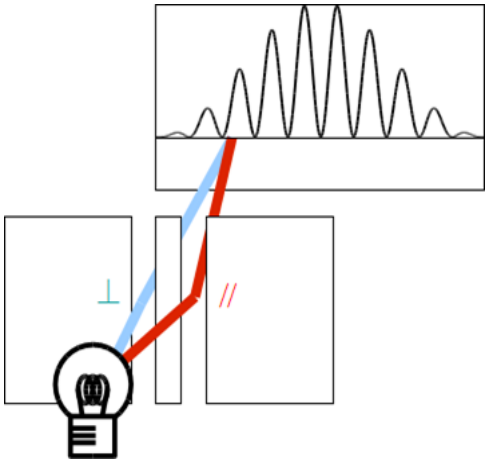

Figure 1-5: Schematic figure of the interference effect in the Young's double slit experiment.

1.2.2 Non-adiabatic transition in dissociation process

The matrix representation of the molecular frame Hamiltonian of a diatomic molecule in the adiabatic electronic basis $|\psi_{n,\Omega}(\vec{r};R)\rangle$ is given as [9–11],

$$
\begin{aligned}
H_{n',\Omega',n,\Omega} &= \delta_{n',n}\delta_{\Omega',\Omega}V_{n,\Omega}(R) - \frac{1}{2\mu R^2}\left\langle \psi_{n',\Omega'} \left| \frac{1}{\sin\theta}\left(\frac{\partial}{\partial\theta} - \mathrm{i}\hat{l}_x\right)\sin\theta\left(\frac{\partial}{\partial\theta} - \mathrm{i}\hat{l}_x\right)\right.\right. \\
&\quad \left.\left. + \frac{1}{\sin^2\theta}\left(\frac{\partial}{\partial\phi} - \mathrm{i}\sin\theta\hat{l}_y - \mathrm{i}\cos\theta\hat{l}_z\right)^2 \right| \psi_{n,\Omega} \right\rangle - \frac{1}{2\mu R}\left\langle \psi_{n',\Omega'} \left| \frac{\partial^2}{\partial^2 R} \right| \psi_{n,\Omega} \right\rangle R \\
&= \delta_{n',n}\delta_{\Omega',\Omega}\left[\frac{1}{2\mu R}\frac{\partial^2}{\partial R^2}R + V_{n,\Omega}(R) + \frac{\hat{\vec{J}}^2 - \Omega^2}{2\mu R^2}\right] \\
&\quad - \delta_{\Omega',\Omega}\left[\frac{1}{\mu}\left\langle \psi_{n',\Omega} \left| \frac{\partial\psi_{n,\Omega}}{\partial R} \right\rangle \frac{1}{R}\frac{\partial}{\partial R}R + \frac{1}{2\mu}\left\langle \psi_{n',\Omega} \left| \frac{\partial^2\psi_{n,\Omega}}{\partial R^2} \right\rangle \right.\right] + H^{\text{Coriolis}}_{n',\Omega',n,\Omega}.
\end{aligned}
\tag{1-12}
$$

Here, Ω denotes the absolute value of the axis component of electronic total angular momentum, $V_{n,\Omega}(R)$ is the adiabatic potential energy of the state $\left|\psi_{n,\Omega}\right\rangle$, ($R$, θ, ϕ) are the ordinary spherical coordinates, $\hat{l}_{x,y,z}$ are respectively the molecular frame x,y,z-components of the total electronic orbital angular momentum. The radial non-adiabatic interaction is characterized by the first-order non-adiabatic coupling terms, $g_{n',\Omega;n,\Omega} \equiv \left\langle \psi_{n',\Omega} \left| \frac{\partial\psi_{n,\Omega}}{\partial R} \right\rangle \right.\cdot \left\langle \psi_{n',\Omega} \left| \frac{\partial^2\psi_{n,\Omega}}{\partial R^2} \right\rangle \right.$ in the last line of equation (1-12) is the second -order non-adiabatic coupling terms, which could be expressed in terms of the first-order non-adiabatic coupling terms as, $\left\langle \psi_{n',\Omega} \left| \frac{\partial^2\psi_{n,\Omega}}{\partial R^2} \right\rangle \right. = \frac{\partial g_{n',\Omega;n,\Omega}}{\partial R} - \sum_k g_{n',\Omega;k,\Omega}g_{k,\Omega;n,\Omega}$, where the effect of the second term is normally negligible [11]. In order to clarify the feature of the radial non-adiabatic interaction, we consider a system consisting of two adiabatic states. In this system, the adiabatic states, ψ_+ and ψ_-, can be converted to diabatic states φ_1 and φ_2 with the angle of the transformation matrix being ϑ, so as to diagonalize the radial momentum $-\mathrm{i}\frac{\partial}{\partial R}$, as [2],

$$\begin{pmatrix} |\varphi_1\rangle \\ |\varphi_2\rangle \end{pmatrix} = \begin{pmatrix} \cos\vartheta & -\sin\vartheta \\ \sin\vartheta & \cos\vartheta \end{pmatrix} \begin{pmatrix} |\psi_+\rangle \\ |\psi_-\rangle \end{pmatrix}, \tag{1-13}$$

$$-\mathrm{i}\left\langle \varphi_2 \left| \frac{\partial \varphi_1}{\partial R} \right\rangle = \mathrm{i}\frac{\partial \vartheta}{\partial R} - \mathrm{i}\left\langle \psi_- \left| \frac{\partial \psi_+}{\partial R} \right\rangle = 0 \rightarrow \frac{\partial \vartheta}{\partial R} = \left\langle \psi_- \left| \frac{\partial \psi_+}{\partial R} \right\rangle \right. \right. \tag{1-14}$$

The matrix representation of the electronic Hamiltonian in the adiabatic basis is diagonal, hence the elements of the electronic Hamiltonian matrix in the diabatic basis H_{11}, H_{22}, H_{12} and conversion angle ϑ satisfy the following equation,

$$\langle \psi_- | \hat{H} | \psi_+ \rangle = H_{12}\cos 2\vartheta + \frac{H_{22} - H_{11}}{2}\sin 2\vartheta = 0 \rightarrow \vartheta = \frac{1}{2}\arctan\left[\frac{2H_{12}}{H_{11} - H_{22}}\right] \tag{1-15}$$

Substituting (1-15) to (1-14) leads to the relationship of the non-adiabatic coupling term and the diabatic basis Hamiltonian elements,

$$\left\langle \psi_- \left| \frac{\partial \psi_+}{\partial R} \right\rangle \right. = \frac{2H_{12}\dfrac{\partial}{\partial R}(H_{11} - H_{22}) + 2\dfrac{\partial H_{12}}{\partial R}(H_{22} - H_{11})}{4H_{12}^2 + (H_{22} - H_{11})^2} \tag{1-16}$$

There are two well-known models for non-adiabatic transition: (1) the Landau-Zener model, which considers the constant diabatic coupling, $H_{12}=A$, and the linear diabatic potentials, $H_{11} = -F_1 R$ and $H_{22} = -F_2 R$, and (2) the Rosen-Zener-Demkov model, which considers the constant diabatic potential difference $H_{22} - H_{11} = \Delta$ and the exponential diabatic coupling, $H_{12} = A\exp(-\alpha R)$. In the two models, one of the two terms of the numerator in equation (1-16) is eliminated. For the Landau-Zener model, the non-adiabatic coupling term has the peak value at the crossing points of diabatic

potentials, $H_{11} = H_{22}$. For the Rosen-Zener-Demkov model, the peak position is at the point, where $\Delta = 2H_{12}$.

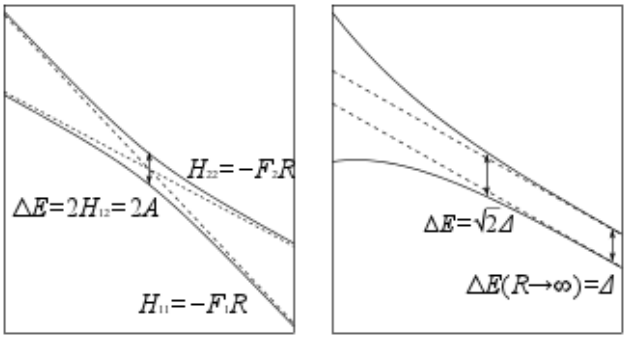

Figure 1-6: Diabatic potential curves (dashed lines) and adiabatic potential curves (solid lines) of the Landau-Zener model (left) and the Rosen-Zener-Demkov model (right). Δ*E* indicates the adiabatic potential difference at the point the non-adiabatic coupling term has the peak value.

The outgoing semi-classical reduced scattering matrix of the Landau-Zener model, is denoted as,

$$O = \begin{pmatrix} e^{-\pi\delta} & -\sqrt{1-e^{-2\pi\delta}}\exp(-i\varphi) \\ \sqrt{1-e^{-2\pi\delta}}\exp(i\varphi) & e^{-\pi\delta} \end{pmatrix}. \qquad (1\text{-}17)$$

where δ is given from the Landau-Zener Formula [12–14], $\delta = \frac{H_{12}^2}{\hbar v(F_1 - F_2)}$, with v and φ being the velocity at the crossing point and the Stokes phase [7,15], respectively. The Stokes phase φ takes the value of $\varphi = \frac{\pi}{4}$ for $\delta = 0$ and $\varphi = \frac{\delta}{12}$ for $\delta >> 1$. The transition probability from the diabatic state 1 to the diabatic state 2 can be interpreted from the above matrix (1-17) as $1 - e^{-2\pi\delta}$. Although this interpretation holds if the initial state consists of a single pure diabatic state, either state 1 or 2 (Figure 1-7 (a) or (b)), the

quantum interference effect must be taken into account if the initial state is a superposition of multiple diabatic states (Figure 1-7 (c) and (d)).

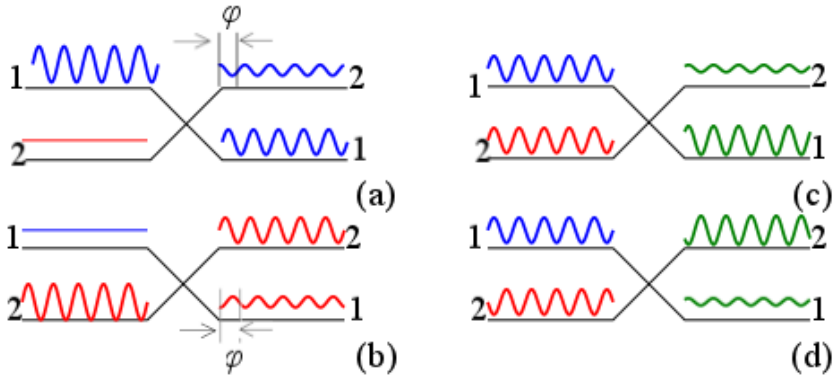

Figure 1-7: Quantum interference scheme having the initial population in (a) diabatic state 1, (b) diabatic state 2, (c) both diabatic states 1, 2 with the same phase, and (d) both diabatic states 1, 2 with phase difference π.

In a real system, the non-adiabatic couplings are seen among multiple states, thus the classification of the non-adiabatic transitions is not straightforward. Moreover, the treatment of non-adiabatic transition as a transition from a single state is not always valid, in which case the proper treatment of the quantum effect and full information during the dissociation process are required.

1.3 Concrete subject of this thesis

ICl molecule is a heteronuclear diatomic halogen molecule without g-u symmetry. The low symmetry of the molecule introduces more avoided crossings among the electronic states with same symmetry $\Delta\Omega=0$, compared to molecules with g-u symmetry,

where avoided crossing exhibits between the states with $\Delta\Omega=0$ and $u \leftrightarrow u/g \leftrightarrow g$. Moreover, the strong spin-orbit coupling of ICl molecule makes photoabsorption to more excited states allowed. Hence, ICl molecule has been a subject of great interest from both experimental and theoretical points of view [16]. Therefore, this molecule is an ideal target molecule for investigating the non-adiabatic transitions in the photodissociation process.

Recent advances in the experimental techniques [17–30] has made it possible to observe the angular momentum polarization of the photofragments, one of the properties required for the 'complete' or 'perfect' experiment [31,32], which inherits the information of the phases of the photofragments' matter wave [33–39], which is much shorter than the ones of electrons due to the heavy rest mass of nuclei. The ab initio calculation with sufficient accuracy is required to compare the theory and experiments. Therefore, the comparison of the theoretical angular momentum polarization, which is described in 2.3, of the photofragments with the experimental ones demonstrates the validity of applying ab initio calculation to evaluation of matter wave phases of the photofragments.

In Chapter 2, the electronic properties of ICl, the linear response theory, the photofragment angular momentum polarization, and the semi-classical treatment of non-adiabatic transitions are reviewed. In Chapter 3, for the purpose of the accuracy assessment for transition dipole moments, those of Cl_2, whose spin-orbit effect is weaker

than those of ICl, were examined in the length-form and in the linear response treatment, including the electronic correlations at various different levels. In Chapter 4, the photodissociation process of ICl in the first absorption band was discussed. The photofragment angular momentum polarization, the anisotropy parameters, and the product branching ratios were calculated with the wave packet propagation method, and were examined in comparison with the experiments. In Chapter 5, the photodissociation process of ICl in the second absorption band was discussed. The anisotropy parameters and the product branching ratios were calculated with three methods, namely, the wave packet propagation method, the semi-classical method, and the classical path method, and were examined in comparison with recent experiments. The author summarizes the results and concludes this thesis in Chapter 6.

Chapter 2
Background of the Study

In this chapter, the author reports the recent studies and theories used in this thesis. The known theoretical properties of the ICl molecule are reviewed in 2.1. A brief explanation of linear response theory and its application is given in 2.2. The formulation of the angular momentum polarization of photofragments is outlined in 2.3. A reinterpretation of the semiclassical reduced scattering matrix is given in 2.4.

2.1 Excited states of ICl molecule

The six valence orbitals of the ICl are denoted σ, π, π*, σ. Due to the larger electronegativity of the Cl atom, the σ and π orbitals correlate to the 3p atomic orbitals of the Cl atom in the dissociation limit, and similarly σ∗ and π∗ orbitals correlate to the 5p atomic orbitals of the I atom (Figure 2-1). While the dominant electronic configuration of the ground electronic state $X(0^+)$ is (2440), where (*pqrs*) denotes the electron occupation number of ($\sigma^p\ \pi^q\ \pi^{*r}\ \sigma^{*s}$), the excited states, which are involved in the first absorption band in the molecular region, have the dominant configuration of one-electron excitation π*→σ*, (2431). The excited states in the second absorption band mostly have the

dominant configuration of one-electron excitation $\pi \rightarrow \sigma^*$, (2341). The correlation diagram is shown in Figure 2-2.

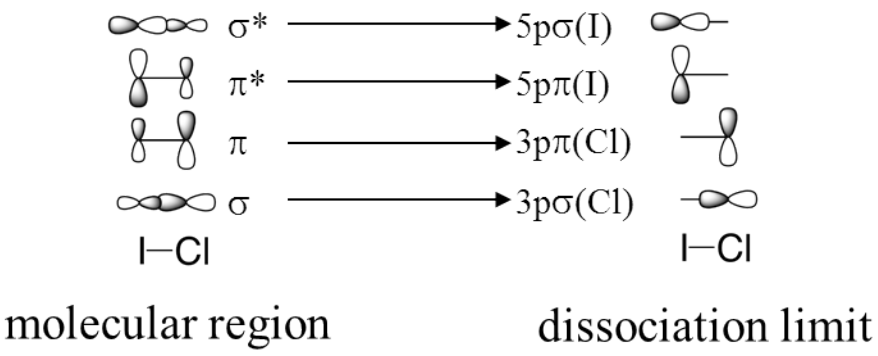

Figure 2-1: Schematic figure of valence orbitals of ICl molecule.

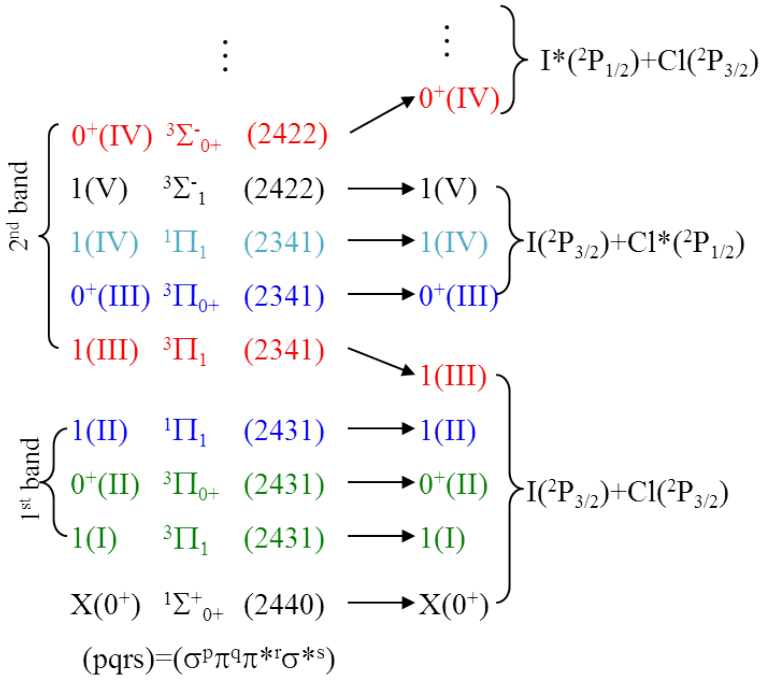

Figure 2-2: Correlation diagram of the ground and excited states of ICl molecule.

Absorption of ICl molecule peaks at 470 nm and 270 nm, in the regions of the first and the second absorption bands, respectively [40]. It is generally believed that the excited states 0^+(II) and 1(I,II) are involved in the first absorption band and the states of 0^+(III,IV) and 1(III,IV,V) are within the second absorption band in the Franck-Condon region. The dissociation channels, whose calculated threshold energies ΔE are below the peak energy of the second absorption band, are as follows:

$$\mathrm{ICl} + h\nu \longrightarrow \mathrm{I} + \mathrm{Cl} \quad \Delta E = 2.17\,\mathrm{eV},$$

$$\longrightarrow \mathrm{I} + \mathrm{Cl}^* \quad \Delta E = 2.29\,\mathrm{eV},$$

$$\longrightarrow \mathrm{I}^* + \mathrm{Cl} \quad \Delta E = 3.10\,\mathrm{eV},$$

$$\longrightarrow \mathrm{I}^* + \mathrm{Cl}^* \quad \Delta E = 3.22\,\mathrm{eV},$$

Hereafter, X($^2P_{3/2}$) and X*($^2P_{1/2}$) are simply denoted as X and X* for X=I, Cl. Let us consider m_J, which is the axis component of electronic total angular momentum for I and Cl. The electronic structure of a non-rotating linear molecule is characterized by Ω value, which is the absolute value of their sum, since Ω value is a conserved property during the axial recoil dissociation. In the dissociation limit, both I and Cl have $m_J = \pm$ 3/2 and $\pm$1/2, there are two $\Omega=0^+$ and three Ω=1 states that correlate to I+Cl, one $\Omega=0^+$ and two Ω=1 states to I+Cl*, one $\Omega=0^+$ and two Ω=1 states to I*+Cl, and one $\Omega=0^+$ and one Ω=1 states to I*+Cl*. Following the labeling of Tonokura et al. [41], the $\Omega=0^+$ and

Ω=1 states are denoted as 0^+(II,III,IV,…) and 1(I,II,III,…), respectively, where the state number is included in the parentheses. The ground state is denoted as X(0^+) exceptionally.

The six valence orbitals σ, π, π*, σ* consist essentially of 5p atomic orbitals of I atom and 3p atomic orbitals of Cl atom. In the Franck-Condon region, the 0^+(II) and 1(I,II) states whose dominant configurations are $^{1,3}\Pi$(2431), both of which are obtained by a single excitation configuration from the ground configuration $^1\Sigma^+$(2440), are involved in the first absorption band. The states, which are involved in the second absorption band, mainly consist of $^{1,3}\Pi$(2342) configurations and $^3\Sigma^-$(2422, 2332) configurations [42]. The large potential energy differences among the 0^+(II) and 1(I,II) states and the wide width of the first absorption band are due to the large exchange integral between the π* and σ* orbitals. For the states involved in the second absorption band, the exchange integral between the π and σ* orbitals is relatively small, hence the potential energy differences among the states are rather small compared to the ones among the states in the first absorption band (Figure 2-3).

In a previous theoretical calculation [42], the squared transition dipole moments from the ground state X(0^+) to the 0^+(II) (with the dominant configuration $^3\Pi$(2431)) and 1(II) (with the dominant configuration $^1\Pi$(2431)) states were calculated as 0.0289 bohr^2 and 0.0209 bohr^2, respectively. The comparable magnitudes of these transition dipole moments were explained with an intensity borrowing mechanism, namely the mixing of the ground state X(0^+) with the spin-free $^3\Pi$(2431) state and the 0^+(II) state with the spin-

free $^1\Sigma^+$(2440). The 0^+(III,IV) states and the 0^+(II,III) states exhibit the avoided crossings Av-1 and Av-2 at the internuclear distances 5.38 bohr and 6.83 bohr, respectively.

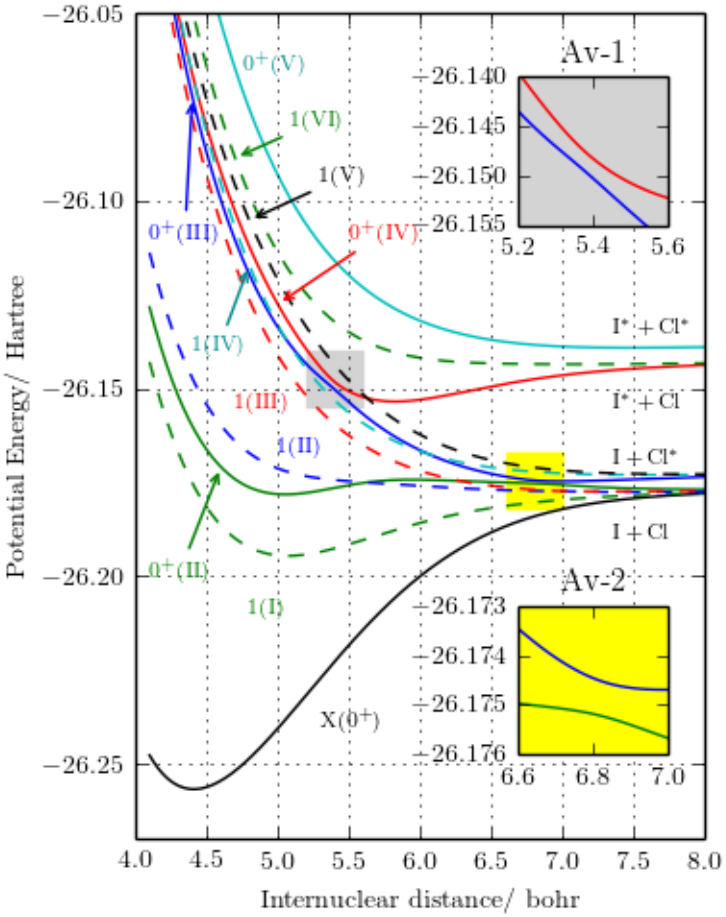

Figure 2-3: Potential energy curves of the X(0^+), 0^+(II-V), and 1(I-VI) states.

2.2 Linear response theory

Here, we consider a field oscillating with the field strength ε and angular frequency ω in the direction of Z-axis to be applied to the molecule system. In analogy with equation (1-1), the perturbation is given as, $\hat{V}(t) = \hat{\mu}_Z \varepsilon \exp(-i\omega t)$, where $\hat{\mu}_Z$ denotes the

Z-component of the dipole moment operator. The system is represented by the time-independent Hamiltonian $\hat{H}_0$ with its eigenstates and eigenenergies denoted as $\left|\psi_{\tilde{n}}^0\right\rangle$ and $E_{\tilde{n}}^0$, and $\left|\psi^0\right\rangle$ and E^0 for the ground state explicitly. The perturbation Hamiltonian $\hat{H}_1(t) = f(t)\hat{V}(t)$ includes the adiabatic switching function *f*, which is initially $(t \to -\infty)$ equal to zero $f(t) \to 0$, and converges to unity $f(t) \to 1$ after the switching $(t \to +\infty)$, to insure the perturbed wave function changes continuously. Let $\left|\psi^0(t)\right\rangle = e^{-iE^0/\hbar}\left|\psi^0\right\rangle$ denote the wave function of the time-dependent Schrödinger equation of the unperturbed system, $i\hbar\frac{\partial}{\partial t}\left|\psi^0(t)\right\rangle = \hat{H}^0\left|\psi^0(t)\right\rangle$. The perturbed system, $i\hbar\frac{\partial}{\partial t}\left|\psi(t)\right\rangle = \hat{H}\left|\psi(t)\right\rangle$, is considered to be initially in the unperturbed state, $\left|\psi(t)\right\rangle = \left|\psi^0(t)\right\rangle (t \to -\infty)$. In the interaction picture $i\hbar\frac{\partial}{\partial t}\left|\psi_I(t)\right\rangle = \hat{H}_I^1\left|\psi_I(t)\right\rangle$, where the corresponding Hamiltonian and wave function are given as, $\hat{H}_I^1 = e^{i\hat{H}^0 t/\hbar}\hat{H}_1(t)e^{-i\hat{H}^0 t/\hbar}$, $\left|\psi_I(t)\right\rangle = e^{i\hat{H}^0 t/\hbar}\left|\psi(t)\right\rangle$, the wave function can be expressed in terms of first-order perturbation expansion as follows,

$$
\begin{aligned}
\left|\psi_I(t)\right\rangle &= \left|\psi^0\right\rangle - \frac{i}{\hbar}\int_{-\infty}^{t}\sum_{\tilde{n}}\left|\psi_{\tilde{n}}^0\right\rangle\left\langle\psi_{\tilde{n}}^0\right|\hat{H}_I(t)\left|\psi^0\right\rangle dt' \\
&= a_0(t)\left[\left|\psi^0\right\rangle - \frac{i}{\hbar}\int_{-\infty}^{t}\sum_{\tilde{n}\neq 0}\left|\psi_{\tilde{n}}^0\right\rangle\left\langle\psi_{\tilde{n}}^0\right|\hat{H}_I(t)\left|\psi^0\right\rangle dt'\right] \\
\left|\psi(t)\right\rangle &= e^{-i\hat{H}^0 t/\hbar}a_0(t)\left[\left|\psi^0\right\rangle - \frac{i}{\hbar}\int_{-\infty}^{t}\sum_{\tilde{n}\neq 0}\left|\psi_{\tilde{n}}^0\right\rangle\left\langle\psi_{\tilde{n}}^0\right|\hat{H}_I(t)\left|\psi^0\right\rangle dt'\right] \\
&= e^{-iE^0 t/\hbar}a_0(t)\left[\left|\psi^0\right\rangle + \sum_{\tilde{n}\neq 0}e^{-i(E_{\tilde{n}}^0 - E^0)t/\hbar}d_{\tilde{n}}(t)\left|\psi_{\tilde{n}}^0\right\rangle\right] \\
&= e^{-iE^0 t/\hbar}a_0(t)\left|\phi(t)\right\rangle.
\end{aligned}
\tag{2-1}
$$

$a_0(t)$ is the coefficient of the "intermediately normalized" wave function $\left|\phi(t)\right\rangle$ [43], hence can also be interpreted as a coefficient of the unperturbed state $\left|\psi^0\right\rangle$. The square of the coefficient $\left|a_0(t)\right|^2 = \left|\left\langle\psi^0\middle|\psi(t)\right\rangle\right|^2$ gives the probability of finding the system in the

unperturbed state $|\psi^0\rangle$. The coefficient $d_{\tilde{n}}(t)$ is for each excited state $|\psi^0_{\tilde{n}}\rangle$. The above wave functions $|\psi(t)\rangle$ are given by perturbation expansion. Therefore, the wave function $|\phi(t)\rangle$ needs to be normalized with the coefficient $a_0(t)$.

The time-dependent Schrödinger equation for the coefficient is given as, $\frac{\partial a_0(t)}{\partial t} = -\frac{\mathrm{i}}{\hbar}\langle\psi^0|\hat{H}^1|\phi(t)\rangle a_0(t)$. By integrating both sides, the phase part of the coefficient $a_0(t)$ is expressed in terms of the quasi-energy $Q(t) \equiv \langle\psi^0|\hat{H}^1|\phi(t)\rangle$ as follows,

$$a_0(t) = \exp\left[-\frac{\mathrm{i}}{\hbar}\int_{-\infty}^{t} Q(t')\mathrm{d}t'\right]. \tag{2-2}$$

Since $a_0(t)$ is the coefficient of time-dependent wave function $|\psi(t)\rangle$, it is apparent the wave function $|\psi(t)\rangle = \exp\left[-\frac{\mathrm{i}}{\hbar}\left(E^0 t + \int_{-\infty}^{t} Q(t')\mathrm{d}t'\right)\right]|\phi(t)\rangle$ propagates in time with $E^0 t + \int_{-\infty}^{t} Q(t')\mathrm{d}t'$. Therefore, the quasi-energy $Q(t)$ represents the energy shift from the unperturbed state $|\psi^0\rangle$ [43–45]. If this wave function is the exact solution of the time-dependent Schrödinger equation, $\mathrm{i}\hbar\frac{\partial}{\partial t}|\psi(t)\rangle = \hat{H}|\psi(t)\rangle$, the Hellmann-Feynman theorem for this wave function leads to the following relation [46],

$$\langle\psi(t)|\frac{\partial\hat{H}(t)}{\partial\varepsilon}|\psi(t)\rangle = \langle\psi(t)|\vec{e}_Z|\psi(t)\rangle\mathrm{e}^{\mathrm{i}\omega t} = \frac{\partial Q(t)}{\partial\varepsilon} + i\frac{\partial}{\partial t}\left\langle\phi(t)\middle|\frac{\partial\phi(t)}{\partial\varepsilon}\right\rangle. \tag{2-3}$$

Since the perturbation is periodic, $\hat{V}(t) = \hat{V}(t + 2\pi/\omega)$, the time-dependent expansion coefficients $d_{\tilde{n}}(t)$, the quasi-energy $Q(t)$ and the second term in equation (2-3) $\frac{\partial}{\partial t}\left\langle\phi\middle|\frac{\partial\phi}{\partial\varepsilon}\right\rangle$ also exhibit the periodicity of $2\pi/\omega$. Therefore, the expansion coefficients and the quasi-energy can be expressed in time-averaged manner as, $d_{\tilde{n}}(\omega) = \frac{\omega}{2\pi}\int_{-\pi/\omega}^{\pi/\omega} d_{\tilde{n}}(t)\mathrm{d}t$, $\{Q\}_T(\omega) = \frac{\omega}{2\pi}\int_{-\pi/\omega}^{\pi/\omega} Q(t)\mathrm{d}t$. The second term in equation (2-3) is a derivative of periodic function, hence the term becomes zero [45], $\left\{\frac{\partial}{\partial t}\left\langle\phi\middle|\frac{\partial\phi}{\partial\varepsilon}\right\rangle\right\}_T(\omega) = 0$. The linear polarizability

$\langle\langle Z,Z\rangle\rangle_\omega$ is given as the field strength derivative of the dipole moment as, $\langle\langle Z,Z\rangle\rangle_\omega \equiv \frac{\partial\{\langle\psi(t)|\hat{\mu}_Z|\psi(t)\rangle\}_T}{\partial\varepsilon} = \left\{\frac{\partial^2 Q(t)}{\partial\varepsilon\partial\varepsilon}\right\}_T$. The linear polarizability $\langle\langle Z,Z\rangle\rangle_\omega$ is the expansion component of the expectation value of the *Z*-component of the dipole moment operator $\hat{\mu}_Z$ in the first-order perturbation as, $\langle\psi(t)|\hat{\mu}_Z|\psi(t)\rangle = \langle\psi^0|\hat{\mu}_Z|\psi^0\rangle + \langle\langle Z,Z\rangle\rangle_\omega \exp(\mathrm{i}\omega t)$. Hitherto, the wave function $|\psi(t)\rangle$ and its time-average have been considered to be the exact solution to the time-dependent Schrödinger equation.

$$\langle\langle Z,Z\rangle\rangle_\omega = \sum_{\tilde{n}} \frac{\partial^2\{Q\}_T}{\partial\varepsilon\partial d_{\tilde{n}}(\omega)} \frac{\partial d_{\tilde{n}}(\omega)}{\partial\varepsilon}. \tag{2-4}$$

In the spectral representation, the above linear response has a singularity for a particular state $\hbar\omega = E^0_{\tilde{n}}$ in the summation, with the corresponding residue being the transition dipole moment for the specific state $\tilde{n}$, $\langle\langle Z,Z\rangle\rangle_\omega = \sum_{\tilde{n}} \frac{\left|\langle\psi^0|\hat{\mu}_Z|\psi^0_{\tilde{n}}\rangle\right|^2}{\omega-\omega_{\tilde{n}}}$ [44,45]. Although the perturbation is essentially required to be Hermitian, $V = V^+$ for the quasi-energy $Q(t)$ to be real, and the inclusion of complex conjugate perturbation $\hat{V}^+ = \hat{\mu}^+_Z\varepsilon^* \exp(\mathrm{i}\omega t)$ introduces the corresponding terms in the general linear response expression, those terms have been omitted in this section for simplicity.

The linear response theory can be applied to the energy functional of averaged quadratic coupled-cluster method, which evaluates the correlation energy with high accuracy by averaging the electron correlation to the extent of including up to quadruply excited configurations [47–53]. The energy functional for the trial function $\tilde{\psi}_{\mathrm{D}}$, which is

in an intermediate normalized form, of the averaged quadratic coupled-cluster method is given as [47,50]

$$E_{\mathrm{corr}}[\tilde{\psi}_{\mathrm{D}}] = \frac{\langle \tilde{\psi}_{\mathrm{D}} | (\hat{H} - E_0) | \tilde{\psi}_{\mathrm{D}} \rangle}{1 + \left(1 - \frac{(n_e - 2)(n_e - 3)}{n_e(n_e - 1)}\right)(\langle \tilde{\psi}_{\mathrm{D}} | \tilde{\psi}_{\mathrm{D}} \rangle - 1)}. \tag{2-5}$$

Here, n_e is the number of electrons. When n_e is below 4 the energy functional is equivalent to the one for the doubly excited configuration interaction method. E_0 is the Hartree-Fock energy of the reference configuration ψ_0, and the trial function is expressed as expansion in terms of the reference configuration ψ_0 and the doubly excited configurations ψ_{cd}^{tu}, as $|\tilde{\psi}_{\mathrm{D}}\rangle = |\psi_0\rangle + \sum_{t<u}^{c<d} c_{cd}^{tu} |\psi_{cd}^{tu}\rangle$. With the corresponding quasi-energy for the averaged quadratic coupled cluster method, the singularity point can be found by solving the eigenvalue problem, which is given as an equation for all pairs of doubly excited configurations *i* and *j*, each of which stands for c_{cd}^{tu} coefficients [45].

$$\sum_{i,j} \frac{\partial^2 E_{\mathrm{corr}}}{\partial c_i \partial c_j} c_i c_j - \omega \delta_{ij} c_i^2 = 0. \tag{2-6}$$

Let the eigenvector matrix of equation (2-6) be U, and the spectral representation of the linear response is given as [45], $\langle\langle Z, Z \rangle\rangle_\omega = \mathrm{Tr}\left[U \frac{|\langle \psi_0 | \hat{\mu}_Z | \psi_{cd}^{tu} \rangle|^2}{E_{corr} - \omega_I \mathbf{1}} U^+ \right]$. The transition dipole moment to the excited state $\tilde{n}$ is given from the residue of the linear response at the singularity point $\omega = \omega_{\tilde{n}}$. Hence by solving the above eigenvalue problem for the energy functional of averaged quadratic coupled-cluster method, one obtains the excitation energy $\omega_{\tilde{n}}$ and the transition dipole moment $\mu_{Z,X\tilde{n}}$, considering the electron correlation to

the extent of including quadruply excited configurations in the averaged quadratic coupled-cluster linear response theory (AQCCLRT) scheme.

2.3 Angular momentum polarization of photofragments

The photofragment A or B of the randomly oriented diatomic molecules AB may exhibit a distribution in its fine structure level population. The author will clarify the connection between this distribution and the transition moment matrix and explain that the transition moment matrix contains the information of the photodissociation process. The angular momentum polarization parameter with rank K and component Q of the photofragment A with momentum $\hbar\vec{k}$ can be given as [35,36,39,54],

$$\left\langle A_{K,Q}\right\rangle(\vec{k},\vec{e}) = \frac{C(K)\sum_{j_A,m_A,m_A'} \frac{\left\langle j_A,m_A'\middle|\hat{j}_Q^{(K)}\middle|j_A,m_A\right\rangle}{\{j_A(j_A+1)\}^{K/2}}\sigma^{j_A}_{m_A',m_A}(\vec{k},\vec{e})}{\sum_{j_A,m_A}\sigma^{j_A}_{m_A,m_A}(\vec{k},\vec{e})}. \tag{2-7}$$

Here, $C(K)$ denotes the normalization constant for each rank K, and $\sigma^{j_A}_{m_A',m_A}(\vec{k},\vec{e})$ denotes the irreducible differential cross-section of the photofragments with light polarization vector $\vec{e}$. The component Q=0 of the parameter $\left\langle A_{K,Q=0}\right\rangle(\vec{k},\vec{e}=\vec{e}_z)$ for linear polarization vector in the +z direction can be interpreted classically as follows: (0) The zeroth rank K=0 is the monopole and takes the value of 1 only, (1) the first rank K=1 parameter ranges from −1 to +1, where −1 and +1 indicates that the classical angular momentum $\vec{j}_A$ is antiparallel and parallel to the +z axis, respectively, (2) the second rank K=2 parameter ranges from −1 to +2, where −1 indicates that $\vec{j}_A$ is perpendicular to the z

axis, and +2 indicates that $\vec{j}_A$ is aligned parallel to the z axis, and so forth. The irreducible differential cross-section of the photofragment A is given in terms of T matrices $\left\langle \Psi^{-(\vec{k})}_{j_A,m_A,j_B,m_B} \left| \hat{\vec{\mu}} \cdot \vec{e} \right| \Psi_{J_1,M_1} \right\rangle$ as follows, where the J_I and M_I denote the initial total angular momentum and the laboratory frame z-component of the J_I vector, respectively,

$$\sigma^{j_A}_{m_A',m_A}(\vec{k},\vec{e}) = \frac{\pi\omega}{\varepsilon_0 c(2J_\mathrm{I}+1)} \sum_{M_1,j_B,m_B} \left\langle \Psi^{-(\vec{k})}_{j_A,m'_A,j_B,m_B} \left| \hat{\vec{\mu}} \cdot \vec{e} \right| \Psi_{J_1,M_1} \right\rangle \left\langle \Psi_{J_1,M_1} \left| \hat{\vec{\mu}} \cdot \vec{e} \right| \Psi^{-(\vec{k})}_{j_A,m_A,j_B,m_B} \right\rangle. \tag{2-8}$$

In the usual experiments, only one of the two photofragments is detected, hence the observation does not yield simultaneous information regarding the both photofragments and the quantum number of the photofragment B is traced out in equation (2-8). Here, $\Psi^{-(\vec{k})}_{j_A,m_A,j_B,m_B}$ denotes the scattering wave function, which satisfies the boundary condition of ingoing spherical wave with various channels and outgoing plane wave with a specific channel [7,9,55], namely, the state with asymptotic wavenumber $\vec{k}$ and electronic total angular momentum of photofragments A and B $\left| j_A, m_A \right\rangle \left| j_B, m_B \right\rangle$, as,

$$\Psi^{-(\vec{k})}_{j_A,m_A,j_B,m_B}(\vec{r},\vec{R}) \xrightarrow{|\vec{R}|\to\infty} \mathrm{e}^{\mathrm{i}\vec{k}\cdot\vec{R}} \left| j_A, m_A \right\rangle \left| j_B, m_B \right\rangle + \sum_{j,j',m'} \left\langle j_A, m_A; j_B, m_B \middle| j, m_A + m_B \right\rangle u_{j',m';j,m_A+m_B}(\vec{R},\vec{k}) \frac{\mathrm{e}^{-\mathrm{i}k'_{j'}|\vec{R}|}}{|\vec{R}|} \left| j', m' \right\rangle. \tag{2-9}$$

The partial-wave expansion of the asymptotic scattering wave function (2-9) leads to the Legendre function expansion of the scattering amplitude $u(\vec{R},\vec{k})$ in the following form,

$$u(\vec{R},\vec{k}) = \frac{1}{2\mathrm{i}\left|\vec{k}\right|}\sum\nolimits_J (2J+1)\mathrm{e}^{2\mathrm{i}\eta_J} P_J(\cos\theta)$$
$$\xrightarrow{J\sin\theta >> 1} \frac{1}{\left|\vec{k}\right|\sqrt{2\pi\sin(\theta)}}\int_0^\infty \sqrt{J}\left[\mathrm{e}^{\mathrm{i}\{2\eta_J-(J+\frac{1}{2})\theta-\frac{\pi}{4}\}} - \mathrm{e}^{\mathrm{i}\{2\eta_J+(J+\frac{1}{2})\theta+\frac{\pi}{4}\}}\right]\mathrm{d}J. \qquad (2\text{-}10)$$

Here, θ denotes the angle between $\vec{R}$ and $\vec{k}$, J denotes the total angular momentum of the dissociating molecule, and the corresponding phase shift is denoted as η_J. The asymptotic form of the Legendre function [56], $P_J(\cos\theta) \sim \sqrt{\frac{2}{\pi J\sin\theta}}\sin\left[\left(J+\frac{1}{2}\right)\theta+\frac{\pi}{4}\right]$, in the limit of $J\sin(\theta) >> 1$, and subsequent replacement of the summation of J with the integration of J lead to the second line of equation (2-10). With application of the stationary phase approximation to the integration, the classical recoiling angle $\gamma = 2\frac{\partial\eta_J}{\partial J}$ (equation (1-6)), in which the scattering amplitude $u(\vec{R},\vec{k})$ has the largest amplitude, is given as, $\gamma = \frac{\pi}{2} - \frac{\delta_J - \delta_{J'}}{J-J'}$ [7,9,57]. Here, δ_J is the phase shift of the elastic scattering wave function in asymptotic region, $\sin(\left|\vec{k}\right|\left|\vec{R}\right| - \frac{\pi J}{2} + \delta_J)$, hence $2\eta_J = \frac{\pi J}{2} - \delta_J$. The total angular momenta J and J' of the final state are limited to the values $J, J' = J_\mathrm{I}, J_\mathrm{I} \pm 1$. Therefore, the separation of the phase shift δ_J from the asymptotic wave function, which weakly depends on the quantum number $J,J'=J_\mathrm{I}\pm 1$ under the condition, simplifies the treatment of the molecular rotation in the dissociation process as [57],

$$\left\langle \Psi_J^{-(\vec{k})}\left|\hat{\vec{\mu}}\cdot\vec{e}\right|\Psi_{J_\mathrm{I}}\right\rangle\left\langle \Psi_{J_\mathrm{I}}\left|\hat{\vec{\mu}}\cdot\vec{e}\right|\Psi_{J'}^{-(\vec{k})}\right\rangle = \mathrm{e}^{\mathrm{i}\gamma(J-J')}\left\langle \Psi_{J_\mathrm{I}}^{-(\vec{k})}\left|\hat{\vec{\mu}}\cdot\vec{e}\right|\Psi_{J_\mathrm{I}}\right\rangle\left\langle \Psi_{J_\mathrm{I}}\left|\hat{\vec{\mu}}\cdot\vec{e}\right|\Psi_{J_\mathrm{I}}^{-(\vec{k})}\right\rangle \qquad (2\text{-}11)$$

While the theoretical calculations are mainly done in the molecular frame, the laboratory frame representation of the irreducible differential cross-section of the

photofragments of equation (2-8) is difficult to evaluate. The dynamical function $f^K(q,q')$, which is the angular momentum polarization parameter represented in the molecular frame, was given by Siebbeles et al. [36],

$$f^K(q,q') = \sum_{j_A,j_B,\Omega_B,\Omega_1,n,n'} (-1)^{2J_1+\Omega_1+K+j_A-\Omega_B+q'} \begin{pmatrix} j_A & j_A & K \\ -\Omega_1 - q + \Omega_B & \Omega_1 + q' - \Omega_B & q - q' \end{pmatrix} C^{n,\Omega_1+q*}_{j_A,\Omega_1+q-\Omega_B;j_B,\Omega_B} C^{n',\Omega_1+q'}_{j_A,\Omega_1+q'-\Omega_B;j_B,\Omega_B} \left\langle \Psi^{-(\vec{k})}_{n',\Omega_1+q'} \middle| \hat{\mu}_{q'} \middle| \Psi_{J_1,\Omega_1} \right\rangle \left\langle \Psi_{J_1,\Omega_1} \middle| \hat{\mu}_{q'} \middle| \Psi^{-(\vec{k})}_{n,\Omega_1+q} \right\rangle \tag{2-12}$$

and related to the irreducible differential cross-section with the application of the high-*J* limit approximation (2-11) as follows [57],

$$\sigma^{j_A}_{m_A',m_A}(\vec{k},\vec{e}) = \frac{3\sigma_0}{4\pi} \sum_{K,q,q',D,Q} (-1)^{j_A-m_A+K+q'} (2K+1)\sqrt{2D+1} E_{D,Q}(\vec{e}) \begin{pmatrix} j_A & j_A & K \\ m_A & -m'_A & m'_A - m_A \end{pmatrix} \begin{pmatrix} 1 & 1 & D \\ q' & q & q-q' \end{pmatrix} D^{K*}_{m_A-m'_A,q-q'}(\vec{k}) D^{D*}_{D,q-q'}(\vec{k}) d^D_{m_A-m'_A,q-q'}(\gamma) \frac{f^K(q,q')}{f^0(0,0)+2f^0(1,1)}. \tag{2-13}$$

Here, q, q', Ω_1 and Ω_B denotes the spherical components of the dipole moment operator $\hat{\vec{\mu}}$ and the molecular frame Z-components of the angular momentum J_1 and j_B, respectively, $E_{D,Q}(\vec{e})$ denotes the transformation matrix of the dipole moment operator $\hat{\vec{\mu}}$ from the molecular frame to the laboratory frame [32,54]. The factor in the brackets $\begin{pmatrix} \bullet & \bullet & \bullet \\ \bullet & \bullet & \bullet \end{pmatrix}$ is a 3-*j* symbol. There is a clear physical meaning to the dynamical functions $f^K(q,q')$: (0) The rank K=0 functions only have the diagonal elements, q=q', and is the parallel and perpendicular excitation components of the photoproduct cross-section for q=q'=0 and q=q'=$\pm$1, respectively, (1) the rank K=1 functions are the orientation of the photoproduct, where the diagonal elements q=q' are the coherent component and the off-diagonal elements $q \neq q'$ are the incoherent component between the parallel and

perpendicular excitation components, (2) and the rank K=2 functions are the alignment of the photoproduct.

2.4 Non-adiabatic transition in semi-classical methods

The semi-classical treatment of the linear crossing problem, namely the Landau-Zener model, without the assumption of constant velocity, gives the semi-classical reduced scattering matrix [7,15], which connects the diabatic amplitudes at the turning point $A_{1,2}(0)$ and the final (positive momentum) amplitudes $A_{1,2}(+\infty)$ as follows,

$$\begin{pmatrix} A_1(+\infty) \\ A_2(+\infty) \end{pmatrix} = \begin{pmatrix} \mathrm{e}^{-\pi\delta} & -\sqrt{1-\mathrm{e}^{-2\pi\delta}}\,\exp(-i\phi) \\ \sqrt{1-\mathrm{e}^{-2\pi\delta}}\,\exp(i\phi) & \mathrm{e}^{-\pi\delta} \end{pmatrix} \begin{pmatrix} A_1(0) \\ A_2(0) \end{pmatrix}, \tag{2-14}$$

where δ is given as [12–14], $\delta = \dfrac{H_{12}^2}{\hbar v(F_1 - F_2)}$, with v, $F_{1,2}$ and H_{12} being the velocity at the crossing point, the slopes of the two linear potentials, and the diabatic coupling matrix element, respectively, and the Stokes phase is denoted as ϕ, However, the above scattering matrix in equation (2-14) does not inherit the sign of the diabatic coupling H_{12}, since it has been explicitly derived for a positive diabatic coupling matrix element H_{12}. The sign of the diabatic coupling H_{12} and the relative phases of the amplitudes $A_{1,2}$ contain ambiguity due to the arbitrary phases of the two diabatic states, hence the sign of the diabatic coupling and the relative phases of the two diabatic states must be conserved in the process of evaluating. The above scattering matrix (2-14) is not applicable to the case, in which the relative phases of the two states are set so that the diabatic coupling

H_{12} has a negative value. The scattering matrix for the negative diabatic coupling matrix element, $H_{12} < 0$, is hereinafter derived following the same procedure as the one for the positive diabatic coupling matrix element, $H_{12} > 0$ [15].

The momentum ($\hbar k$) representation of the equations for the linearly crossing two diabatic states are given as,

$$\begin{aligned}\left[\frac{(\hbar k)^2}{2\mu} - E - \mathrm{i}F_1\frac{\partial}{\partial k}\right]u_1(k) &= -H_{12}u_2(k),\\ \left[\frac{(\hbar k)^2}{2\mu} - E - \mathrm{i}F_2\frac{\partial}{\partial k}\right]u_2(k) &= -H_{12}u_1(k).\end{aligned} \tag{2-15}$$

Here, $F_{1,2}$ denotes the slope of the two linear potentials, $V_{1,2} = -F_{1,2}R$, with $F_1 > F_2$, and we consider the diabatic coupling H_{12} as a constant negative value. Elimination of $u_2(k)$ in equation (2-15), in which we change the variables as in equation (2-16), leads to the simplified differential equation (2-17) for the amplitude of the state 1.

$$\begin{cases} t = -\dfrac{2H_{12}}{F}k, \\ a^2 = -\dfrac{\hbar^2 F\Delta F}{16\mu H_{12}^3}, \\ b^2 = -\dfrac{E\Delta F}{2H_{12}F}, \\ u_i(t) = \sqrt{\dfrac{\hbar^2}{\mu F_i}}\exp\left[\dfrac{\mathrm{i}}{2}\sqrt{1+\dfrac{4F^2}{\Delta F^2}}(b^2 t - a^2 t^3/3)\right]B_i(t), \\ F = \sqrt{F_1 F_2}, \quad \Delta F = F_1 - F_2, \end{cases} \tag{2-16}$$

$$\begin{aligned} &\frac{\partial^2 B_1}{\partial t^2} + K(t)B_1 = 0, \\ &K(t) = \frac{1}{4} + \mathrm{i}a^2 t + \frac{1}{4}\left(a^2 t^2 - b^2\right)^2. \end{aligned} \tag{2-17}$$

The asymptotic condition for the amplitude B_1, $\left|\dfrac{\mathrm{d}}{\mathrm{d}t}\dfrac{1}{\sqrt{K(t)}}\right| << 1$, is analogous to the semi-classical condition in ordinary position representation. Specifically, if $\dfrac{1}{\sqrt{K(t)}}$ varies slowly as the function of dimensionless variable, t, the asymptotic form of the amplitude is given as, $B_1 \propto \exp(\pm\mathrm{i}\int\sqrt{K}\,\mathrm{d}t)$. In the high energy limit, $b^2 >> 1$, the condition is satisfied for $t \to \pm\infty$ and $t = 0$, and the corresponding asymptotic forms are given as,

$$
\begin{aligned}
B_1 \overset{t\to\pm\infty}{\sim} & B_1(\pm\infty)\left(\frac{b/a-t}{b/a+t}\right)^{-\mathrm{i}\delta}\exp\left[-\frac{\mathrm{i}}{2}\left(\frac{a^2t^3}{3}-b^2t\right)\right] \\
& + \frac{B_2(\pm\infty)}{2(a^2t^2-b^2)}\left(\frac{b/a-t}{b/a+t}\right)^{\mathrm{i}\delta}\exp\left[\frac{\mathrm{i}}{2}\left(\frac{a^2t^3}{3}-b^2t\right)\right], \\
B_1 \overset{t\to 0}{\sim} & B_1(0)\left(\frac{t-b/a}{t+b/a}\right)^{-\mathrm{i}\delta}\exp\left[-\frac{\mathrm{i}}{2}\left(\frac{a^2t^3}{3}-b^2t\right)\right] \\
& + \frac{B_2(0)}{2(a^2t^2-b^2)}\left(\frac{t-b/a}{t+b/a}\right)^{\mathrm{i}\delta}\exp\left[\frac{\mathrm{i}}{2}\left(\frac{a^2t^3}{3}-b^2t\right)\right].
\end{aligned}
\tag{2-18}
$$

The given asymptotic forms break down at the singularity point, $t = \pm b/a = \pm\dfrac{H_{12}\sqrt{8\mu E}}{\hbar F}$, hence, in order to connect the asymptotic functions above, t is linearly expanded, $t = \pm b/a + \tau$, in the vicinity of the point. Here, we explicitly derive the scattering matrix, which connects the turning point and outgoing amplitudes, $A_{1,2}(0)$ and $A_{1,2}(+\infty)$, respectively. However, since the diabatic coupling is negative, the approximate function, which connects the two amplitudes, is the one at the singularity point, $t = -b/a = -\dfrac{H_{12}\sqrt{8\mu E}}{\hbar\sqrt{F}}$. Therefore, equation (2-17) is transformed into the form of the Weber equation [58], whose solution is given by the parabolic cylinder functions (or the Weber functions), as,

$$
\frac{\mathrm{d}^2B_1}{\mathrm{d}\tau^2} + \left(\frac{1}{4} - \mathrm{i}ab + a^2b^2\tau^2\right)B_1 = 0, \tag{2-19}
$$

Upon connection of the general solution of equation (2-19) to the asymptotic forms (2-18) and substitution of the amplitude, $B_1 = A_1\exp\left[-\dfrac{\mathrm{i}}{2}\left(\dfrac{a^2t^3}{3}-b^2t\right)\right]$, the reduced scattering matrix for the negative diabatic coupling H_{12} is derived as,

$$\begin{pmatrix} A_1(+\infty) \\ A_2(+\infty) \end{pmatrix} = \begin{pmatrix} \mathrm{e}^{-\pi\delta} & \sqrt{1-\mathrm{e}^{-2\pi\delta}}\exp(\mathrm{i}\phi) \\ -\sqrt{1-\mathrm{e}^{-2\pi\delta}}\exp(-\mathrm{i}\phi) & \mathrm{e}^{-\pi\delta} \end{pmatrix} \begin{pmatrix} A_1(0) \\ A_2(0) \end{pmatrix}. \tag{2-20}$$

It is apparent from equations (2-14) and (2-20) that the off-diagonal element of the reduced scattering matrix must be determined from the sign of the diabatic coupling H_{12}. If the diabatic coupling is negative, $H_{12} < 0$, the transformation angle ϑ in equation (1-13) is taken to be zero at the turning point, hence $A_-(0) = A_2(0), A_+(0) = A_1(0)$ and $A_-(+\infty) = A_1(+\infty), A_+(+\infty) = -A_2(+\infty)$, the reduced scattering matrix in adiabatic representation, where A_- and A_+ denote the amplitudes of the lower and higher adiabatic states, is given as,

$$\begin{pmatrix} A_-(+\infty) \\ A_+(+\infty) \end{pmatrix} = \begin{pmatrix} \sqrt{1-\mathrm{e}^{-2\pi\delta}}\exp(\mathrm{i}\phi) & \mathrm{e}^{-\pi\delta} \\ -\mathrm{e}^{-\pi\delta} & \sqrt{1-\mathrm{e}^{-2\pi\delta}}\exp(-\mathrm{i}\phi) \end{pmatrix} \begin{pmatrix} A_-(0) \\ A_+(0) \end{pmatrix}. \tag{2-21}$$

The scattering matrix (2-21) is in analogy with the ones given by Nakamura [10,59,60]. Although the inelastic transition probability, derived from the scattering matrix for either positive or negative diabatic coupling, is given as [7,10], $4\mathrm{e}^{-2\pi\delta}(1-\mathrm{e}^{-2\pi\delta})\sin^2\phi$, the author emphasizes that the arbitrariness of the diabatic coupling sign is only valid for evaluation of transition probability in full collision processes. For a half-collision process, specifically photodissociation process, the reduced scattering matrix, which is consistent with the relative phase of the states, must be chosen with a special care.

Chapter 3
Calculation Method Dependence of Transition Dipole Moments

3.1 Introduction

The numerical instability of the transition dipole moments calculated in a limited configuration interaction scheme [61–63] has been an unresolved obstacle to theoretical study of the photoexcitation process. Cl_2 molecule is one of the cases. In this chapter, the author examines the theoretical transition dipole moment of Cl_2, whose spin-orbit effect is weaker than those of ICl, in the length form and the linear response treatment, including the electronic correlations at various different levels. A significant dependence of the transition dipole moments on the one-electron orbitals used in the calculation was clarified from the analysis.

3.2 Calculation method

The author used aug-ccpVQZ for the basis functions of Cl atom. Three types of molecular orbitals were employed: (1) The ordinary closed shell (… $5\sigma_g^2\ 2\pi_u^4\ 2\pi_g^4\ 5\sigma_u^0$) self-consistent field molecular orbitals (denoted as SSSCF, the abbreviation of state

specific self-consistent field), (2) the state-averaged self-consistent field (SASCF) molecular orbitals, which are optimized for the ensemble average energy for all the configurations derived from $(5\sigma_g\ 2\pi_u\ 2\pi_g\ 5\sigma_u)^{10}$, and (3) the state-averaged multi-configuration self-consistent field (SAMCSCF) molecular orbitals for which the average energy of the $X^1\Sigma^+_g(5\sigma_g^2\ 2\pi_u^4\ 2\pi_g^4\ 5\sigma_u^0)$ and $C^1\Pi_u(5\sigma_g^2\ 2\pi_u^4\ 2\pi_g^3\ 5\sigma_u^1)$ states with equal weight for each state (including the degeneracy factor of two for the $C^1\Pi_u$ state). Here, $5\sigma_g$, $2\pi_u$, $2\pi_g$, and $5\sigma_u$ orbitals essentially consist of 3p atomic orbitals of Cl atoms. The spin-orbit interaction was not included in this chapter's calculation. For each type of molecular orbitals, the SCI, SDCI and AQCCLRT calculations were carried out. The singlet configuration state functions were generated with the reference of $(5\sigma_g\ 2\pi_u\ 2\pi_g\ 5\sigma_u)^{10}$. For the SCI calculation, all the singly excited configuration state functions from these reference configuration state functions were included in the first-order configuration interaction scheme. Similarly for the SDCI calculation, all the singly and doubly excited configuration state functions from the reference configuration state functions were included in the second-order configuration interaction scheme. From the multi-reference SCI, SDCI wave functions, the author calculated the excitation energy, the transition density matrix and the transition dipole moment in the length form from the ground state $X^1\Sigma^+_g$ to the excited state $C^1\Pi_u$. For the multi-reference AQCCLRT, the excitation energy and the transition dipole moment were calculated. All the electronic

state calculations were performed with the COLUMBUS program package (5.9.2) [64]. The internuclear distance was fixed at 3.76 bohr for all the calculation.

3.3 Results and discussion

3.3.1 Transition dipole moment in the length form

The transition dipole moments (TDMs) calculated (Table 3-1) in length form with SSSCF-MRAQCCLRT, SASCF-MRSDCI, and SAMCSCF-MRSDCI were largely underestimated compared to the experiment [65]. From the analysis of the weight of the dominant CSF of the calculated $X^1\Sigma^+_g$ and $C^1\Pi_u$ state wave functions (Table 3-2), it is apparent that the $C^1\Pi$ state has a low weight of the dominant CSF. Hence, the error of the transition dipole moment and the excitation energy calculated with SSSCF-MRAQCCLRT was due to the selection of the SSSCF-MO, which was not appropriate to the $C^1\Pi$ state.

Table 3-1: Theoretical transition dipole moments from the $X^1\Sigma^+_g$ state to the $C^1\Pi$ state. LF: Calculation in length form. R: Calculation in response treatment. [a] The experimental data was taken from [65].

	ΔE/ Hartree	TDM(LF)/ bohr	TDM(R)/ bohr
Expt.[a]	0.1381	0.140	
SSSCF-MRSCI	0.1402	0.146	0.102
SSSCF-MRSDCI	0.1885	0.149	0.164
SSSCF-MRAQCCLRT	0.1168	---	0.0287
SASCF-MRSCI	0.1408	0.132	0.0758
SASCF-MRSDCI	0.1456	0.0268	0.0851
SASCF-MRAQCCLRT	0.1411	---	0.119
SAMCSCF-MRSCI	0.1425	0.122	---
SAMCSCF-MRSDCI	0.1468	0.0235	---
SAMCSCF-MRAQCCLRT	0.1425	---	0.114

Table 3-2: Weight of the dominant CSFs of the $X^1\Sigma^+_g$ and $C^1\Pi$ states.

	$X^1\Sigma^+_g$	$C^1\Pi$
SSSCF-MRSCI	0.958611	0.785843
SSSCF-MRSDCI	0.880977	0.831682
SSSCF-MRAQCCLRT	0.832253	0.446053
SASCF-MRSCI	0.931354	0.918410
SASCF-MRSDCI	0.869265	0.855501
SASCF-MRAQCCLRT	0.824969	0.805619
SAMCSCF-MRSCI	0.932687	0.918446
SAMCSCF-MRSDCI	0.870241	0.855766
SAMCSCF-MRAQCCLRT	0.825803	0.805485

The transition dipole moment $\mu_{x,X^1\Sigma^+_g,C^1\Pi_x}$ in the length form is calculated using the dipole integrals $\langle\varphi_i|x|\varphi_j\rangle$ and the transition density matrix $\Gamma^{X^1\Sigma^+_g,C^1\Pi_x}_{i,j}$,

$$\mu_{x,X^1\Sigma^+_g,C^1\Pi_x} = \sum_{i,j}\langle\varphi_i|x|\varphi_j\rangle\Gamma^{X^1\Sigma^+_g,C^1\Pi_x}_{i,j}. \quad (3\text{-}1)$$

For the SASCF-MRSDCI and SAMCSCF-MRSDCI calculations, the dipole integrals $\langle\varphi_i|x|\varphi_j\rangle$ of equation (3-1) is the same as the ones for the SASCF-MRSCI and SAMCSCF-MRSCI, respectively, thus the error of the transition dipole moments

originates from the transition density matrix $\Gamma_{i,j}^{X^1\Sigma_g^+, C^1\Pi_x}$. The molecular orbitals included in the calculation consist of 168 orbitals ($22\times\sigma_{(g,u)}$, $15\times\pi_{(x,y)(g,u)}$, $11\times\delta_{(xy,x^2-y^2)(g,u)}$, $5\times\varphi_{(x(3x^2-y^2),y(3y^2-x^2))(g,u)}$), hence there are 1650 symmetrically allowed transition density matrix elements for the dipole operator *x* (B_{3u}). Among those elements of the transition density matrix of the SASCF-MRSDCI and SAMCSCF-MRSDCI calculations, the ones, whose differences are larger than 0.01 from the matrix elements of the SASCF-MRSCI and SAMCSCF-MRSCI, respectively, are tabulated in Table 3-3.

Table 3-3: Elements of transition density matrices whose differences between the matrices of MRSCI and MRSDCI are larger than 0.01. The correlating atomic orbitals are indicated in the parentheses.

SASCF-MRSCI, MRSDCI	SAMCSCF-MRSCI, MRSDCI
$5\sigma_g(3p)$, $4\pi_{xu}(3d)$	$5\sigma_g(3p)$, $4\pi_{xu}(3d)$
$5\sigma_g(3p)$, $6\pi_{xu}(4d)$	$5\sigma_g(3p)$, $6\pi_{xu}(4d)$
$12\sigma_g(4d)$, $2\pi_{xu}(3p)$	$12\sigma_g(4d)$, $2\pi_{xu}(3p)$
$2\pi_{yu}(3p)$, $2\delta_{xyg}(4d)$	$5\sigma_u(3p)$, $2\pi_{xu}(3p)$

The element, whose corresponding dipole integral magnitude is the largest, is the ($5\sigma_g(3p)$, $4\pi_{xu}(3d)$) element. The dipole integrals of this element are 0.665 and 0.656 bohr for the SASCF and SAMCSCF, respectively.

In order to examine the effect of the $4\pi_u$ orbital, the calculations with the reference of $(5\sigma_g\ 2\pi_u\ 2\pi_g\ 5\sigma_u\ 4\pi_u)^{10}$ were carried out (Table 3-4). The $4\pi_u(3d)$ orbital can be considered as an orbital, which polarizes the $2\pi_u(3p)$ orbital. Hence, inclusion of this one-electron orbital to the reference space improved the excitation energy and the transition dipole moment of the SSSCF-MRAQCCLRT, as Table 3-4 shows closer

agreement with the experiment than the ones in Table 3-1. Although the transition dipole moments of the SASCF-MRSDCI and SAMCSCF-MRSDCI calculations have also been improved, the ones of the SASCF-MRSCI and SAMCSCF-MRSCI showed better agreement with the experiment and numerical stability.

Table 3-4: Theoretical transition dipole moments from the $X^1\Sigma^+_g$ state to the $C^1\Pi$ state with extended reference space of $(5\sigma_g\ 2\pi_u\ 2\pi_g\ 5\sigma_u\ 4\pi_u)^{10}$. The values in the parentheses shows the difference from the ones with reference space of $(5\sigma_g\ 2\pi_u\ 2\pi_g\ 5\sigma_u)^{10}$ (Table 3-1). [a] The experimental data was taken from [65].

	ΔE/ Hartree	TDM/ bohr
Expt.[a]	0.1381	0.140
SSSCF-MRSCI	0.1541 (+0.0139)	0.150 (+0.004)
SSSCF-MRSDCI	0.1781 (−0.0104)	0.143 (−0.007)
SSSCF-MRAQCCLRT	0.1504 (+0.0436)	0.0927 (+0.0640)
SASCF-MRSCI	0.1453 (+0.0045)	0.148 (+0.016)
SASCF-MRSDCI	0.1484 (+0.0028)	0.0676 (+0.0408)
SASCF-MRAQCCLRT	0.1473 (+0.0062)	0.0992 (−0.020)
SAMCSCF-MRSCI	0.1470 (+0.0045)	0.115 (−0.007)
SAMCSCF-MRSDCI	0.1502 (+0.0034)	0.0754 (+0.0519)
SAMCSCF-MRAQCCLRT	0.1478 (+0.0053)	0.121 (+0.007)

3.3.2 Linear response treatment

The transition dipole moment can be approximately evaluated with the CI coefficients C_K^I and the transition density matrix Γ_{ij}^{IJ} as

$$\mu_{x,I,J} = (E_J - E_I)\left[\sum_K C_K^I \frac{\partial C_K^J}{\partial \varepsilon_x} + \sum_{i,j}\left\langle \varphi_i \left| \frac{\partial \varphi_j}{\partial \varepsilon_x} \right\rangle \Gamma_{ij}^{IJ}\right.\right]. \tag{3-2}$$

The author notes that the equation (3-2) is only valid for the MCSCF wave function or complete CI wave function [44,61–63]. The theoretical transition dipole

moment in response treatment for SSSCF-MRSCI, SSSCF-MRSDCI, SASCF-MRSCI, and SASCF-MRSDCI wave functions are given in Table 3-1. On the contrary to the ones of the SSSCF calculations, the SASCF calculations have shown a stability in the contributions of the first term, the CI-term, and the second term, MO-term, in square brackets of equation (3-2), in that the MRSCI and MRSDCI gave similar values (Table 3-5). It also shows the theoretical transition dipole moment approaches the experimental value as the level of the electronic correlation taken into account becomes higher. Although improvement in the theoretical transition dipole moment with SASCF was seen as calculation level became higher, the results in length form with MRSCI calculation remained to be in better agreement with the experiment.

Table 3-5: Contribution of the CI-term and MO-term of the transition dipole moment calculations.

	CI-term/ bohr	MO-term/ bohr	TDM/ bohr	MO-term contribution
SSSCF-MRSCI	0.161	−0.0595	0.102	−58.6 %
SSSCF-MRSDCI	0.0575	0.107	0.164	65.0 %
SSSCF-MRAQCCLRT	---	---	(0.0287)	---
SASCF-MRSCI	0.0493	0.0265	0.0758	35.0 %
SASCF-MRSDCI	0.0552	0.0299	0.0851	35.2 %
SASCF-MRAQCCLRT	---	---	(0.119)	---

3.4 Conclusion

The author examined the theoretical transition dipole moment of Cl_2 from the ground state $X^1\Sigma^+_g$ to the excited state $C^1\Pi_u$ calculated with various methods. The theoretical transition dipole moment in linear response treatment exhibited numerical stability of the

contribution from the CI-term and MO-term for SASCF one-electron orbital. The transition dipole moment in length form with MRSCI calculation showed better agreement with the experiment than the ones of the MRAQCCLRT, which includes the electronic correlation to the extent of including quadruply excited configurations.

Chapter 4
Photodissociation Process of ICl in the First Absorption Band

4.1 Introduction

Samartzis and Kitsopoulos observed the product fraction [Cl*]/ ([Cl]+[Cl*]) and the anisotropy parameter β in the almost entire wavelength region of 400-570 nm [66]. They considered the non-adiabatic transition probability p_2 between the 0^+(II,III) states at Av-2 is equivalent to the product fraction [Cl*]/([Cl]+[Cl*]) with the assumption that dissociation process takes place only on the Ω=0^+ states. The product fraction [Cl*]/([Cl]+[Cl*]) they observed showed qualitative agreement with the theoretical transition probability given by de Vries et al. [67] in the wavelength region of 480-530 nm. For the anisotropy parameter β of the I+Cl channel, they observed a sharp decrease of the parameter in the wavelength region shorter than 480 nm. From the results, they have suggested the contribution of a new state with Ω=1 symmetry with its potential energy higher than the 0^+(II) state in the Franck-Condon region.

Rakitzis et al. observed the angular momentum polarization parameters in the wavelength region of 490-560 nm [23]. They later analyzed the parameters, expressed in

terms of $(1-f_1)$, $(1-f_2-f_3)$, and f_3, which are the branching fractions from the 0^+(II) to X(0^+), the one from the 1(I) state to the 1(II) state, and the one from 1(I) state to the 1(III) state, respectively, and the anisotropy parameter β [68]. The parameter Im[$a^{(1)}{}_1$(//,⊥)] was expressed as,

$$\begin{aligned}\mathrm{Im}[a_1^{(1)}(//,\perp)] = \frac{1}{\sqrt{5}}\sqrt{(\beta+1)(2-\beta)}[&\sqrt{f_1 f_2}\sin(\phi_{0+(\mathrm{II})}-\phi_{1(\mathrm{I})}) \\ &-\sqrt{(1-f_1)f_3}\sin(\phi_{\mathrm{X}(0+)}-\phi_{1(\mathrm{III})}) \\ &+\sqrt{\frac{2(1-f_1)(1-f_2-f_3)}{3}}\sin(\phi_{\mathrm{X}(0+)}-\phi_{1(\mathrm{II})}) \\ &-\sqrt{\frac{2f_1(1-f_2-f_3)}{3}}\sin(\phi_{0+(\mathrm{II})}-\phi_{1(\mathrm{II})})].\end{aligned} \tag{4-1}$$

They calculated the branching fractions f_n from the angular momentum polarization parameters obtained from the experiment, with an assumption that the potential energy difference between the same Ω symmetry be negligibly small after the avoided crossings, hence asymptotic phase differences ($\phi_I - \phi_J$) between the same Ω symmetry were considered to be zero. The asymptotic phase differences between the different Ω symmetry were calculated with semi-classical equation using the *ab initio* potential energy curves of reference [42]. For example, the asymptotic phase difference between the X and Y states, whose avoided crossing is at $R_{X,Y}$, was evaluated as

$$\phi_X - \phi_Y = \int_{R_{X,Y}}^{\infty}\{k_X(R)-k_Y(R)\}\mathrm{d}R. \tag{4-2}$$

Here, $k_X(R)$ is the wavenumber of the X state. With the calculated branching fractions f_1=0.04, f_2=0.12, and f_3=0.49, they have concluded the *ab initio* potential energy curves needs correction especially in the long-range. The author of this thesis notes, however,

they have neglected the Stokes phase [7,10,15] upon evaluating the phase differences, and the previous work [69] has shown the Stokes phase has significant influence on the parameter $\mathrm{Im}[a^{(1)}_1(//,\perp)]$. In this chapter, the photofragment angular momentum polarization, the anisotropy parameters, and the product branching ratios were calculated with the wave packet propagation method, and were examined in comparison with the experiments.

4.2 Computational methods

The relativistic effective core potentials, by Christiansen, Ermler and their co-workers [70,71] with the valence shells being 5s5p for I atom and 3s3p for Cl atom, have been used for the calculation. For the basis functions, cc-pVTZ by Peterson et al. [72] for I atom and cc-pVTZ by Woon and Dunning [73] for Cl atom have been used. The sets of five primitives (α_s(I)=0.02075, α_p(I)=0.01344, α_d(I)=0.03180, α_f(I)=0.08410, and α_g(I)=0.4739) and (α_s(Cl)=0.02364, α_p(Cl)=0.01390, α_d(Cl)=0.04500, α_f(Cl)=0.1380, and α_g(Cl)=0.8270) were added to the I and Cl basis sets, respectively. The basis sets have been optimized by Ohnishi [69] so as the dissociation energies of the $X(0^+)$ and 1(I) states show the best agreement with the spectroscopic data [74]. The state-averaged self-consistent field molecular orbitals, which are optimized for the ensemble average energy [75] for all the configurations derived from $(\sigma, \pi, \pi^*, \sigma^*)^{10}$, namely 10 electrons in the six valence orbitals, which essentially consist of 5p atomic orbitals of I atom and 3p

atomic orbitals of Cl atom, have been employed. For the spin-orbit configuration interaction calculations, singlet and triplet configuration state functions (CSFs) were generated with the reference of $(\sigma, \pi, \pi^*, \sigma^*)^{10}$. All the singly and doubly excited CSFs from these reference CSFs were included in the second-order configuration interaction (CI) scheme. The continuities of the CI wave functions as functions of internuclear distance R were kept throughout the whole region. From the CI wave functions, the author calculated potential energy curves and non-adiabatic coupling terms taking into account both CI and MO term contributions. The Davidson correction was included in the CI energy. For the transition dipole moments, the spin-orbit CI method in the first-order CI scheme was used. All the electronic state calculations were performed with the COLUMBUS program package [76].

The wave packet method was used to study the dissociation dynamics. The time propagations of the wave packets were carried out with Chebychev expansion method [77–79]. The calculation was done for the bond distances of 3.00~27.20 bohr segmented with 4096 grids. The first- and second-order non-adiabatic interactions were implemented in the wave packet propagation program by the author of this thesis to perform calculation including multiple electronic states (up to eight states). The second-order non-adiabatic interaction was evaluated with the first-order non-adiabatic coupling terms [11]. The wave packet program has been modified from the original one [80], which was

designed to calculate for single adiabatic excited state, written by Balint-Kurti et al. The atomic masses employed were $^{127}I^{35}Cl$.

With a spin-orbit CI method, symmetry of the molecular electronic state is denoted as Ω, the absolute value of the molecular axis component of the total electronic angular momentum. Radial non-adiabatic transition can occur only between electronic states with same Ω ($\Delta\Omega$=0). Axial recoil approximation is generally valid for the photodissociation of ICl in the first absorption band, since the recoil velocity of the direct dissociation is much faster than the rotational speed. From this reason, the molecular rotation effect, such as a Coriolis non-adiabatic transition during the dissociation process is not considered, and the ground state molecules are assumed to be randomly oriented.

The angular momentum polarization parameter $\mathrm{Im}[a_1^{(1)}(//,\perp)]$ of Cl, which Rakitzis et al. observed [23], can be expressed in terms of the dynamical functions $f^K_{q,q'}$, which are defined as in equation (2-12), of rank K [37], introduced by Siebbeles et al. [36] as

$$\mathrm{Im}[a_1^{(1)}(//,\perp)] = 3(2j_A+1)\frac{\mathrm{Im}[f^1_{1,0}]}{f^0_{0,0}+2f^0_{1,1}}. \qquad (4\text{-}3)$$

The total angular momentum j_A of the photofragment Cl is 3/2, in this case. The dynamical functions of zeroth rank (scalar quantity) in the denominator of the right hand side of equation (4-3), is proportional to photofragment's cross-section, hence the first rank dynamical function in the numerator characterizes the essential part of this angular momentum polarization parameter. The T matrix elements were calculated with time-

dependent wave packet method [80]. When the T matrix element of the Franck-Condon electronic state $\tilde{n}$ and asymptotic electronic state n is written in terms of the amplitude $r_{\tilde{n},n}$ and the asymptotic phase $\phi_{\tilde{n},n}$ as

$$\left\langle \Psi^{-(J_i)}_{\tilde{n},\Omega_i+q,n} \middle| \mu_{\tilde{n},q} \middle| \Psi^{J_i}_{\Omega_i} \right\rangle = r_{\tilde{n},n} \exp(i\phi_{\tilde{n},n}), \tag{4-4}$$

${r_{\tilde{n},n}}^2 \Big/ \sum_m {r_{\tilde{n},m}}^2$ $(\tilde{n} \neq n)$ can be interpreted as the non-adiabatic transition probability from the state $\tilde{n}$ to the state n.

The zeroth rank dynamical functions ${f^{\theta}}_{0,0}$ and ${f^{\theta}}_{1,1}$ in equation (4-3) have only contributions of the two T matrix elements with the same asymptotic electronic states n=n', and represent incoherent dissociation processes, whose values are actually proportional to the photofragment cross-sections. On the other hand, the first rank dynamical function ${f^{\lambda}}_{1,0}$ has the contribution of the two T matrix elements of q=1 (perpendicular) and q=0 (parallel). For example, when the contributions of the T matrix elements of 0^+(II)→0^+(II) and 1(I)→1(I) are dominant, the phase of the dynamical function ${f^{\lambda}}_{1,0}$ can be ultimately written as $\phi_{0+(II),0+(II)} - \phi_{1(I),1(I)}$, which describes the difference of quantum mechanical phase shifts between the states 0^+(II) and 1(I). This indicates that the angular momentum parameter Im[${a_1}^{(1)}(//,\perp)$] represents the coherence of T matrix elements with electronic states of different Ω.

The initial Franck-Condon wave packets were generated for the four excited Ω=0^+ states (0^+(II), 0^+(III), 0^+(IV), 0^+(V)) and the five excited Ω=1 states (1(I), 1(II), 1(III), 1(IV), 1(V)) with the corresponding transition dipole moments and the ground

vibrational state of the parent molecule. The wave packets were propagated on these nine excited states and the ground state $X(0^+)$, including the radial non-adiabatic interactions among all the states, and the photofragmentation T matrix elements were obtained. Due to the restricted numbers of grids, the calculated T matrix elements showed small oscillation near thresholds (Figure 5, 7, 8). This oscillation is to be considered of numerical error rather than of physical phenomena.

4.3 Results and discussion

4.3.1 Adiabatic potential energy curves of ICl

The calculated adiabatic potential energy curves are shown in Figure 2-3. Here, the $X(0^+)$, 1(I), 0^+(II), and 1(II) states adiabatically correlate to I+Cl products. Spectroscopic constants were determined using the Fourier grid Hamiltonian method by Balint-Kurti et al. [5,80]. The calculation was done for the bond distances of 3.00~27.20 bohr segmented with 4096 grids. For the $X(0^+)$, 1(I), and 0^+(II) states, vibrational levels v''=0~9, v''=0~35, and v''=0~2 were included, respectively, for these calculations. These levels were taken to match with experimental fitting procedure by Pardo et al. [74]. These spectroscopic constants of the $X(0^+)$, 1(I), and 0^+(II) states are shown in Table 1, and are in reasonable agreement with the experimental values. The author thus expects that quantitative results can be obtained for the photodissociation process in the Franck-Condon region with these ab initio potential energy curves.

Table 4-1: Spectroscopic constants of the $X(0^+)$, 1(I), and 0^+(II) states. Experimental values are taken from Pardo et al. [74].

	r_e/ bohr	r_e(exp.[a])/ bohr	ω_e/ cm^{-1}	ω_e(exp.[a])/ cm^{-1}	$\omega_e\chi_e$/ cm^{-1}	$\omega_e\chi_e$(exp.[a])/ cm^{-1}
$X(0^+)$	4.4106	4.3858	383.74	384.30	1.307	1.501
1(I)	5.0701	5.0877	212.0	210.3	1.06	1.50
0^+(II)	5.0527	5.0267	216.3	211.4	5.34	7.98

4.3.2 Absorption spectra, polarization parameters, and non-adiabatic transition probabilities

In the numerical calculation of the absorption cross sections, the author used the program by Balint-Kurti et al. [5]. The calculated absorption spectra are shown in Figure 4-1, and are in fair agreement with experimental data by Seery et al. [40], implying that the transition dipole moments, used in this calculation, have reasonable accuracy.

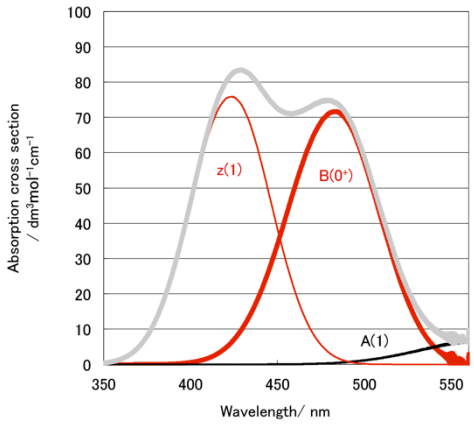

Figure 4-1: Absorption spectra in the first band. Thick red line for the absorption to the 0^+(II) state (denoted as B(0^+)), thin black line for the 1(I) state (denoted as A(1)), and thin red line for the 1(II) state (denoted as z(1)). Thick grey line shows total absorption spectrum.

Rakitzis et al. examined the polarization parameter in the 490 nm~560 nm region [23]. In this region, parallel transition is dominated by the excitation to the 0^+(II) state and perpendicular one by the excitation to the 1(I) state. After a parallel transition to the 0^+(II) state, the Franck-Condon wave packet will propagate to the dissociation limits of the 0^+(III) or X(0^+) state through non-adiabatic transitions, or to the dissociation limit of the 0^+(II) state adiabatically. In the case of a perpendicular transition to the 1(I) state, the Franck-Condon wave packet will propagate to the dissociation limits of the 1(III) or 1(II) state, or to the dissociation limit of the 1(I) state adiabatically. As shown in Figure 4-2, non-adiabatic transition occur between the 0^+(II) and 0^+(III) states at 6.8 bohr, between the X(0^+) and 0^+(II) states at 9.1 bohr, between the 1(II) and 1(III) states at 6.8 bohr, and

between the 1(I) and 1(II) states at 8.6 bohr. Note that the non-adiabatic interactions of $X(0^+)$/ 0^+(II) and 1(I)/ 1(II) cannot be recognized from their potential energy curves alone.

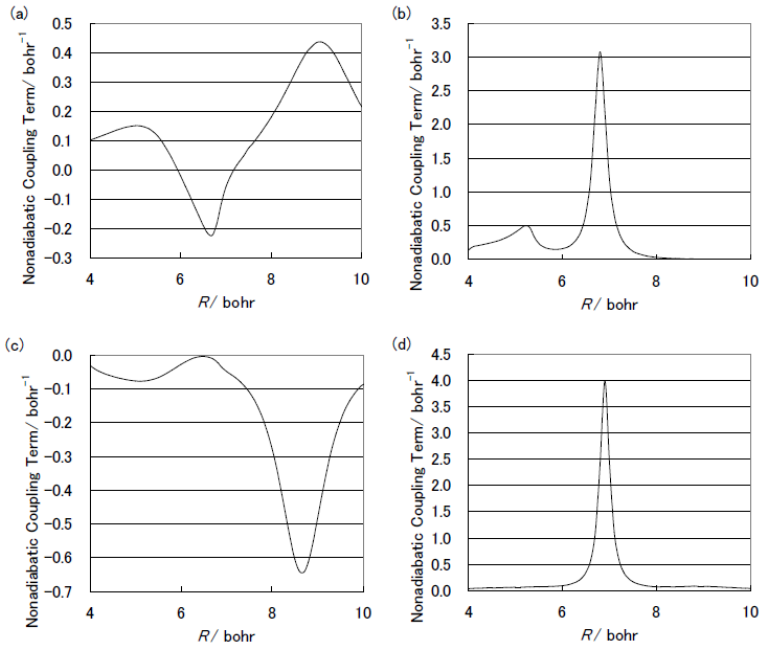

Figure 4-2: First-order non-adiabatic coupling terms between (a) $X(0^+)$ and 0^+(II) states, (b) 0^+(II) and 0^+(III) states, (c) 1(I) and 1(II) states, and (d) 1(II) and 1(III) states.

The calculation of non-adiabatic transition probabilities after the parallel transition is shown in Figure 4-3. The result was about 50%, while Alexander and Rakitzis estimated that a large portion (96 %) of the wave packet will propagate to the $X(0^+)$ state. The 0^+(III) state adiabatically correlates to the I+Cl* products, and does not contribute to the polarization parameter of Cl. The non-adiabatic transition probabilities from the 1(I) state to the 1(II) and 1(III) states are shown in Figure 4-4. The results were about 70% and 10% respectively, and show qualitative agreement with the result of Alexander and Rakitzis (49 % and 12 %).

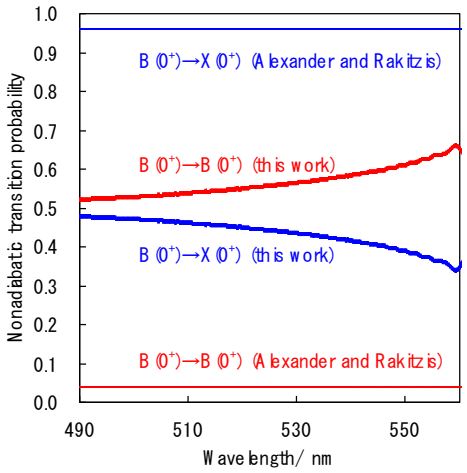

Figure 4-3: Non-adiabatic transition probability from the 0^+(II) state (denoted as B(0^+)) to the X(0^+) state. Thick lines: Wave packet method. Thin lines: Transition probability estimated by Alexander and Rakitzis [68]. Red lines: Probability which the electronic state remains on the 0^+(II) state. Blue lines: Transition probability from the 0^+(II) state to the X(0^+) state.

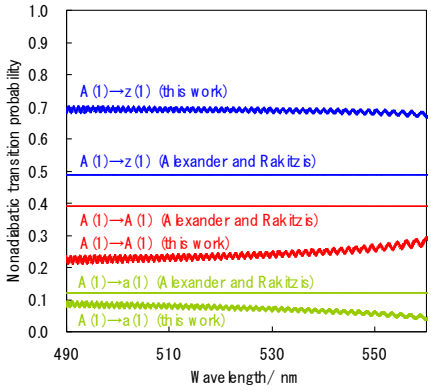

Figure 4-4: Non-adiabatic transition probability from the 1(I) state (denoted as A(1)) to the 1(II) and 1(III) states (denoted as z(1) and a(1), respectively). Thick lines: Wave packet method. Thin lines: Transition probability estimated by Alexander and Rakitzis [68]. Red lines: Probability which the electronic state

remains on the 1(I) state. Blue lines: Transition probability from the 1(I) state to the 1(II) state. Green lines: Transition probability from the 1(I) state to the 1(III) state.

Alexander and Rakitzis [68] estimated the non-adiabatic transition probabilities from the angular momentum polarization data of Cl, which Rakitzis et al. [23] obtained experimentally. When only the 1(I) and 0^+(II) states dominantly contribute to this parameter in the observed wavelength region, by separating the T matrix element into the amplitude $r_{\tilde{n},n}$ and the phase $\phi_{\tilde{n},n}$ as in (4-4), the polarization parameter can be approximately given as [68]

$$\mathrm{Im}\left[a_1^{(1)}(//,\perp)\right] \propto r_{0+(\mathrm{II}),0+(\mathrm{II})} r_{1(\mathrm{I}),1(\mathrm{I})} \sin\left(\varphi_{0+(\mathrm{II}),0+(\mathrm{II})} - \varphi_{1(\mathrm{I}),1(\mathrm{I})}\right) \tag{4-5}$$

The amplitude of this parameter can be considered as the geometric average of $r^2_{0+(\mathrm{II}),0+(\mathrm{II})}$ and $r^2_{1(\mathrm{I}),1(\mathrm{I})}$. The square of $r_{0+(\mathrm{II}),0+(\mathrm{II})}$ is the probability of the 0^+(II) state Franck-Condon wave packet that propagated to the dissociation limit without non-adiabatic transition, while the square of $r_{1(\mathrm{I}),1(\mathrm{I})}$ being the probability of the 1(I) state Franck-Condon wave packet that propagated to the dissociation limit without non-adiabatic transition. As the amplitude in (4-5) is given as a geometric average of $r^2_{0+(\mathrm{II}),0+(\mathrm{II})}$ and $r^2_{1(\mathrm{I}),1(\mathrm{I})}$, it will be at the largest when these two probabilities are approximately the same. The phase part in equation (4-5) can be expressed as the difference of quantum mechanical phase shifts between the 0^+(II) and 1(I) states. These phase shifts are very sensitive to the potential energy curves. The theoretical calculation of this polarization parameter is shown in Figure 4-5 and is in quantitative agreement with the results of Rakatzis et al. implying

that the potential energy curves used in this calculation was in high accuracy. Note that the envelope of the oscillation has a maximum around at 530-540 nm.

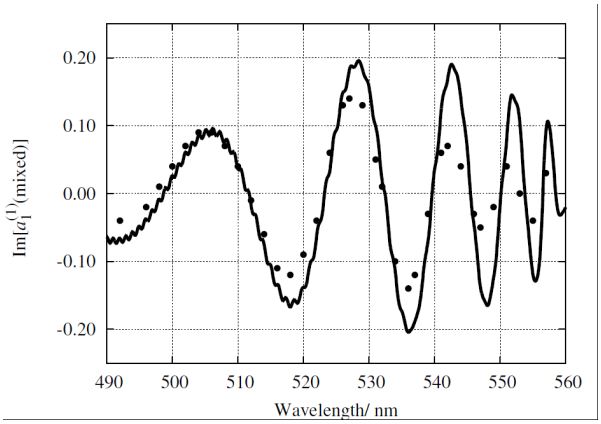

Figure 4-5: First-rank angular momentum polarization parameter. Solid line: Wave packet method. Dots: Experiment by Rakitzis et al. [23]. Correction of the data was made by Alexander and Rakitzis in [68].

Samartzis and Kitsopoulos examined the product fraction of Cl* for each wavelength between 400-570 nm [66]. The product fraction, which was called curve crossing probability in their paper, was evaluated with following formula, regardless of angular distribution,

$$P = [\mathrm{Cl}^*]/([\mathrm{Cl}] + [\mathrm{Cl}^*]). \tag{4-6}$$

They first assumed the product fraction P defined above would represent the non-adiabatic transition probability from the 0^+(II) state to the 0^+(III) state. Since both the 0^+(II) and X(0^+) states correlate to Cl product and the 0^+(III) state correlates to Cl* product, and the avoided crossing between the 0^+(II) and 0^+(III) states exists before the one between the 0^+(II) and X(0+) states, the product fraction can represent approximately the non-adiabatic transition probability from the 0^+(II) state to the 0^+(III) state under axial

recoil approximation. Strictly speaking, however, the product fraction could be expressed in terms of photoabsorption cross sections $\sigma(1(\mathrm{I}))$, $\sigma(0^+(\mathrm{II}))$, and $\sigma(1(\mathrm{II}))$ from the $X(0^+)$ state to the 1(I), 0^+(II), and 1(II) states, respectively, and the non-adiabatic transition probability p_2 from the 0^+(II) state to the 0^+(III) state, as

$$P = \frac{\sigma(0^+(\mathrm{II}))p_2}{\sigma(1(\mathrm{I})) + \sigma(0^+(\mathrm{II})) + \sigma(1(\mathrm{II}))}. \tag{4-7}$$

Therefore, their assumption holds and $P=p_2$, only when $\sigma(1(\mathrm{I}))$ and $\sigma(1(\mathrm{II}))$ are negligibly small. As Figure 4-1 indicates, however, photoproducts from perpendicular transition would be observed in higher wavelengths and lower wavelengths due to the presence of the 1(I) and 1(II) states, respectively. Hence, the product fraction is not equivalent to non-adiabatic transition probability in this broad wavelength region, and the effect of the $\Omega=1$ states cannot be neglected, as Samartzis and Kitsopoulos finally concluded. In this study, the author calculated the above product fraction theoretically from the photofragmentation (not photoabsorption) cross sections for the respective product channels using the wave packet method described above, including the five $\Omega=0^+$ states and the five $\Omega=1$ states. The photofragmentation cross sections for the respective product channels are the absolute square of T matrix elements.

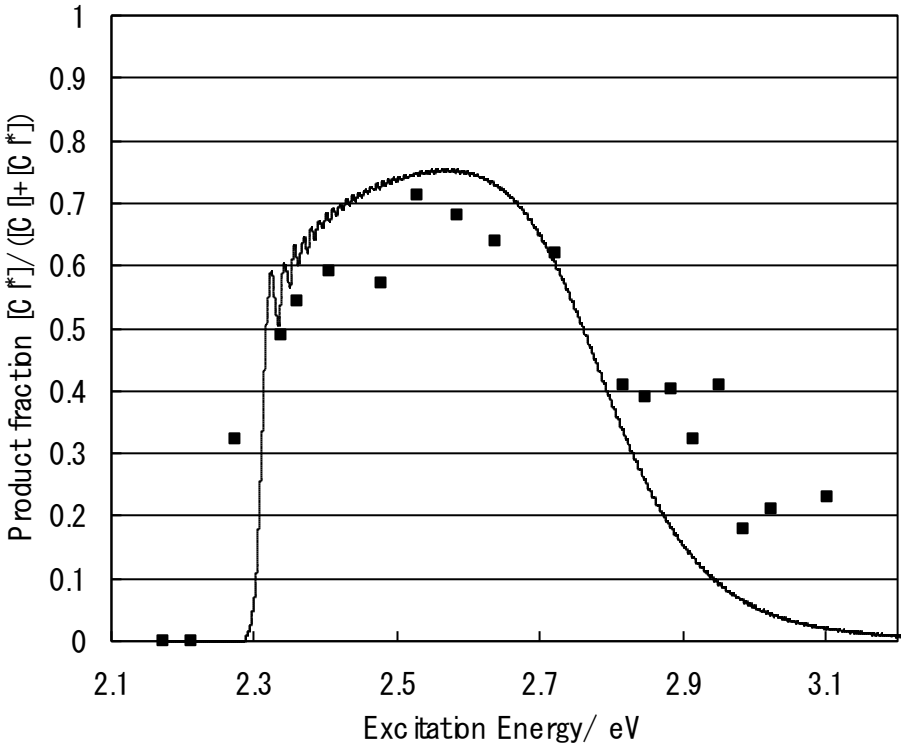

Figure 4-6: Product fraction of Cl*. Solid line: Wave packet method. Dots: Experiment by Samartzis and Kitsopoulos [66].

The result of the product fraction in Figure 4-6, is in a quantitative agreement with the result of Samartzis and Kitsopoulos [66]. The 1(I) and 1(II) states adiabatically correlate to the asymptotic limit I+Cl and have negligible NACTs with the 1(IV) and 1(V) states correlating to I+Cl*. Hence the decrease of product fraction *P* in the higher energy region could be explained from the large absorption cross section of the 1(II) state. Although the absorption cross section of the 1(I) state is relatively small, it also contributes to decrease of the product fraction *P*.

Samartzis and Kitsopoulos also examined the anisotropy parameter β in the region of 400-570 nm. In this wide wavelength region, photoabsorption to the 1(II) state, as well as the 1(I), 0^+(II) states can occur, therefore the β parameter for Cl changes drastically. The calculation result in Figure 4-7 shows qualitative agreement with the experimental data. They speculated that there exists an Ω=1 state in the energy region higher than the 0^+(II) state, from the decrease in photodissociation product Cl* and from the β parameter in the higher energy region, and named the C state as a candidate. From the theoretical calculations of this study, the author affirmed that, the known A(1) and z(1) states [81,82] are the only possible Ω=1 states, that are responsible for the first absorption band, and from the above analysis, their speculated Ω=1 state turns out to be the z(1) state.

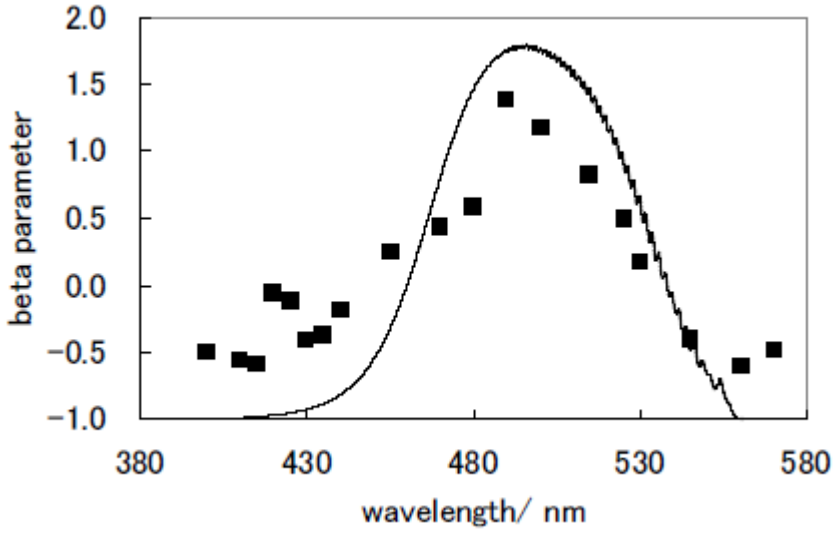

Figure 4-7: Anisotropy parameter of β photofragment Cl. Solid line: Wave packet method. Dots: Experiment by Samartzis and Kitsopoulos [66].

It is interesting to point out that at 530-540 nm (2.3-2.4 eV), the envelope of the oscillation has a maximum (Figure 4-5), the product fraction of Cl* becomes 1/2 (Figure 4-6), and the β parameter for Cl becomes 0 (no anisotropy, Figure 4-7). This is of course not coincident, since the interference between the parallel and perpendicular components is expected to be most significant when these two probabilities become identical.

4.3.3 Non-adiabatic transition between the X(0^+) and 0^+(II) states

As shown in Figure 4-3, a significant non-adiabatic transition probability between the X(0^+) and 0^+(II) states was also estimated by Alexander and Rakitzis [68]. The NACT between these states in Figure 4-2(a) shows a maximum value at 9.1 bohr, where a hidden avoided crossing exists. When the electronic wave functions of the X(0^+) state are expanded with CSFs and plotted as a function of the internuclear distance R as shown in Figure 4-8, the most dominant CSFs are $^1\Sigma^+(1441)$ and $^1\Sigma^+(2332)$, with the occupation number notation of $(pqrs)\equiv(\sigma^p\pi^q\pi^{*r}\sigma^{*s})$. These σ, π, π^*, and σ^* orbitals are localized respectively to σ(Cl3p), π(Cl3p), π(I5p), and σ(I5p) in these asymptotic regions. As R is increased, the most dominant CSF for the X(0^+) state is switched from $^1\Sigma^+(1441)$ to $^1\Sigma^+(2332)$ at the avoided crossing region, suggesting the non-adiabatic transition between the X(0^+) and 0^+(II) states is of Landau-Zener type.

The PECs of the X(0^+) and 0^+(II) states in Figure 2-3 do not clearly exhibit the avoided crossing, although its existence at 9.1 bohr can be confirmed from the maximum

point of NACTs. Hence, inclusion of the NACTs is essential to the quantitative calculation of non-adiabatic transition probabilities, especially at longer bond distance regions. The quantum mechanical approach includes the effect of the NACTs and also the quantum mechanical interference effects among the several dissociation paths. Although the non-adiabatic transition probability from the 0^+(II) state to the X(0^+) state does not show a quantitative agreement with the simulated result of Alexander and Rakitzis [68], the angular momentum parameter Im[$a_1^{(1)}$(//,⊥)] itself shows a qualitative agreement with the experimental result of Rakitzis et al. [23]. Hence, the potential energy curves obtained in this work were considered accurate enough to give the parameter Im[$a_1^{(1)}$(//, ⊥)] with quantitative agreement with the experimental result of Rakitzis et al.

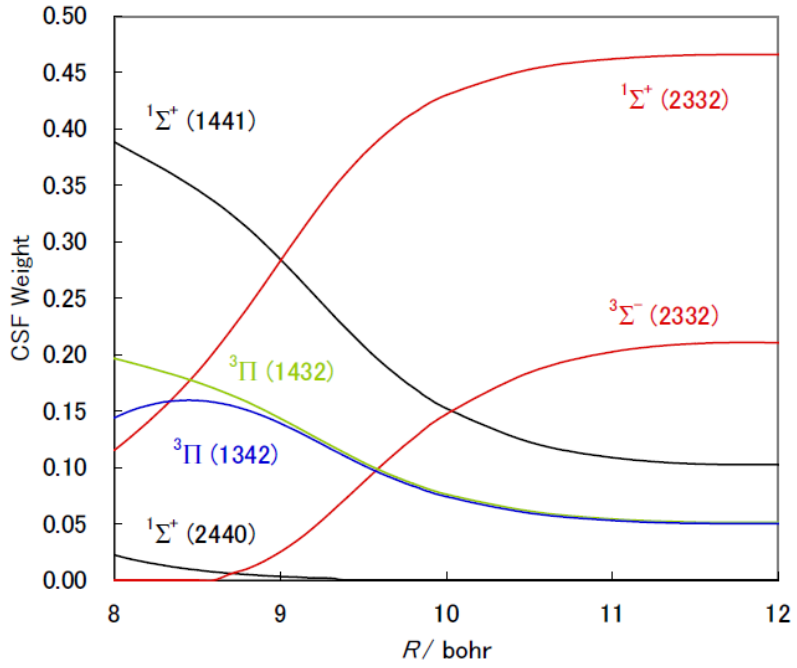

Figure 4-8: Weight of configuration state functions (squared CI coefficients) of the X(0^+) state. The interchange of the dominant configuration state functions could be found around the point where an avoided crossing between the X(0+) and 0^+(II) states exists.

4.4 Conclusions

The low-lying excited states of ICl, and calculated the product branching ratio, the anisotropy parameter β, and the first-rank angular momentum parameter Im[a1(1)(//,⊥)] were obtained with ab initio method. The calculation result of the product fraction and the β parameter supported the experimental analysis by Samartzis and Kitsopoulos [66], and the indicated obscure state turned out to be the z(1) state. For the first-rank angular momentum parameter Im[a1(1)(//,⊥)], the high accuracy of the potential energy curves, obtained in this study, was affirmed from quantitative agreement of phase part with

experimental data by Rakitzis et al. [23]. The non-adiabatic transitions between the $X(0^+)$ and $0^+(II)$ states is of an Landau-Zener type without apparent avoided crossing between the two potential energy curves.

Chapter 5
Photodissociation Process of ICl in the Second Absorption Band

5.1 Introduction

The branching ratios following the excitation to the second absorption band have been investigated by Tonokura et al. by analyzing the Doppler profiles of the photofragments [41]. In their theoretical study, they obtained the squared transition dipole moments from the ground X(0^+) state to the 0^+(III), 1(IV), and 0^+(IV) states as $\mu^2_{0+(III)}$=0.0220 bohr^2, $\mu^2_{1(IV)}$=0.0232 bohr^2, and $\mu^2_{0+(IV)}$=0.00696 bohr^2, respectively, and the non-adiabatic transition probabilities at the avoided crossings Av-1 and Av-2 as p_1=0.77 and p_2=0.90, respectively. The branching ratios of the I+Cl, I+Cl*, and I*+Cl channels were calculated as 18, 46, 36 %, respectively, using the equation

$$\frac{[\mathrm{I}+\mathrm{Cl}]}{[\mathrm{I}+\mathrm{Cl}]+[\mathrm{I}+\mathrm{Cl}^*]+[\mathrm{I}^*+\mathrm{Cl}]} = \frac{(1-p_1)p_2\mu^2_{0+(\mathrm{II})}+p_1p_2\mu^2_{0+(\mathrm{IV})}}{\mu^2_{0+(\mathrm{II})}+\mu^2_{1(\mathrm{IV})}+\mu^2_{0+(\mathrm{IV})}}, \tag{5-1}$$

$$\frac{[\mathrm{I}+\mathrm{Cl}^*]}{[\mathrm{I}+\mathrm{Cl}]+[\mathrm{I}+\mathrm{Cl}^*]+[\mathrm{I}^*+\mathrm{Cl}]} = \frac{(1-p_1)(1-p_2)\mu^2_{0+(\mathrm{II})}+p_1(1-p_2)\mu^2_{0+(\mathrm{IV})}+\mu^2_{1(\mathrm{IV})}}{\mu^2_{0+(\mathrm{II})}+\mu^2_{1(\mathrm{IV})}+\mu^2_{0+(\mathrm{IV})}}, \tag{5-2}$$

$$\frac{[\mathrm{I}^*+\mathrm{Cl}]}{[\mathrm{I}+\mathrm{Cl}]+[\mathrm{I}+\mathrm{Cl}^*]+[\mathrm{I}^*+\mathrm{Cl}]} = \frac{p_1p_2\mu^2_{0+(\mathrm{II})}+(1-p_1)p_2\mu^2_{0+(\mathrm{IV})}}{\mu^2_{0+(\mathrm{II})}+\mu^2_{1(\mathrm{IV})}+\mu^2_{0+(\mathrm{IV})}}. \tag{5-3}$$

The author notes that they have not included the contribution of the quantum interference between the 0^+(III,IV) states in the above calculation. Although their experiment indicated that the I+Cl channel products were dominated by parallel transition components, later ion imaging experiment by Rogers et al. [83] showed their contributions were negligibly small in the I+Cl channel. Moreover, two other experiments by Jung et al. and Cheng et al. also indicated that the I+Cl channel products were dominated by perpendicular transition components at the wavelength of 304.67 nm [84,85]. However, since the theoretical transition dipole moment to the 0^+(IV) state, which diabatically correlates to the I+Cl channel, was calculated to have a comparable magnitude to the one to the 0^+(III) state, Rogers et al. considered that the theoretical transition dipole moment to the 0^+(III) state could be overestimated and they also questioned the existence of the avoided crossing Av-1 [83].

Diamantopoulou et al. have also observed the fine structure branching ratio in a wider region of the second absorption band [86]. Regarding the photoabsorption at wavelength of 235 nm, their result of perpendicular transition component for dissociation channel I+Cl* is similar to those of Rogers et al. [83]. Their study also indicates a very small contribution of the dissociation channel I+Cl compared to the dissociation channel I*+Cl. More importantly, by analyzing the experimental results, the anisotropy parameter β of the I+Cl channel shows a strong photon energy dependence, which implies comparable contribution of parallel and perpendicular transitions for this channel. For the

perpendicular transition, the 1(III) state is the only state which adiabatically correlates to the I+Cl channel, hence the contribution of the 0^+(III,IV) states to this channel should be comparable to the 1(III) state. In this chapter, the anisotropy parameters and the product branching ratios were calculated with three methods, namely, the wave packet propagation method, the semi-classical method, and the classical path method, and were examined in comparison with recent experiments.

5.2 Computational methods

Most of the calculations were carried out with the same method as previous Chapter 4, with the following exceptions. The calculations were carried out by the 'contracted spin-orbit configuration interaction' method [87], where the total Hamiltonian including the spin-orbit part is diagonalized in the basis of the lower-lying spin-free configuration interaction eigenstates of $^{1,3}(2\times\Sigma^+,\Sigma^-,2\times\Pi,\Delta)$, all of which correlate with the ground state atomic dissociation limit of I(^{2}P)+Cl(^{2}P). The phases of the configuration interaction wave functions of the relevant states were fixed at the Franck-Condon region, so that both of the transition dipole moments $\mu_{0+(III)}$ and $\mu_{0+(IV)}$ from the ground state X(0^+) have positive values. For the transition dipole moments, the uncontracted SOCI method in the first-order CI scheme has been used. All the electronic structure calculations were performed with the COLUMBUS program package [76].

For the purpose of CI wave function analysis, the electronic structure calculation with MOs transformed into atomic orbital (AO)-like orbitals [88] were also performed. The unitary transformations were restricted for the pairs of the valence orbitals (σ, σ^*), (π_x, π_x^*), and (π_y, π_y^*) within the reference orbital subspace, so that the overlaps of MO with the one at dissociation limit become maximum. Note that the configuration space formed from these transformed AO-like orbitals is identical to the one with the original MOs.

5.3 Results and discussion

5.3.1 The second absorption band spectra

The present results for the transition dipole moments (Figure 5-1) were not significantly different from those in the previous work [42]. The result of the total absorption spectrum is in agreement with the one observed by Seery and Britton (Figure 5-2) [2]. The absorption cross section of the 1(III) state, which correlates to the dissociation channel I+Cl, is very small compared to the ones of the 0^+(III,IV) states.

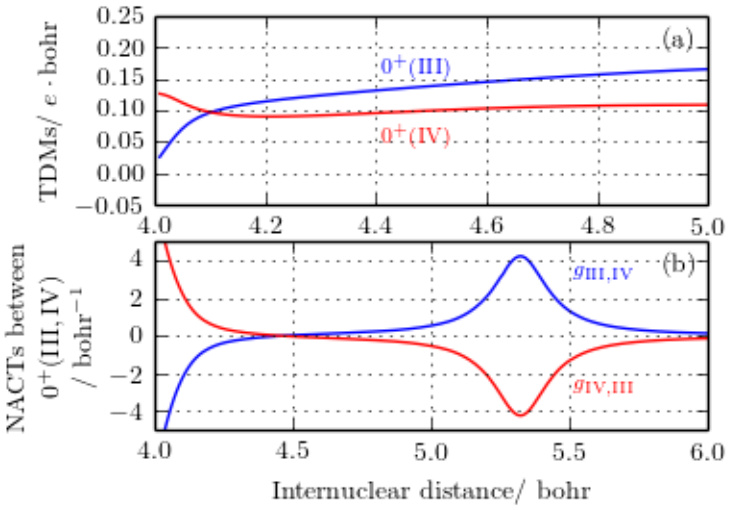

Figure 5-1: (a) Calculated transition dipole moments to the states 0^+(III) and 0^+(IV), and (b) non-adiabatic coupling terms between 0^+(III,IV).

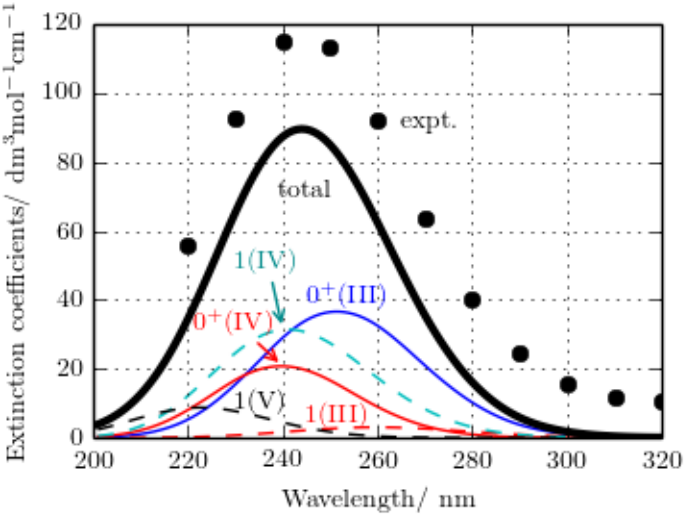

Figure 5-2: Theoretical absorption spectra of the second absorption band. Thin solid lines represent $\Omega=0^+$ states, dashed lines $\Omega=1$ states, and thick solid line total sum of the theoretical calculation. Dots represent experimental values by Seery and Britton [40].

Figure 5-1 shows the magnitudes of the calculated transition dipole moments to the 0^+(III,IV) states are in the same order. Due to the strong spin-orbit interaction, the

spin-orbit coupled adiabatic states ψ are linear combinations of the spin-free states ϕ. With the 'contracted SOCI' method in the Franck-Condon region, each of the adiabatic states of $X(0^+)$, and 0^+(III,IV) was approximately described in terms of the dominant spin-free states as

$$\psi_{X(0+)} \approx 0.988\times\phi(^1\Sigma^+(2440)) + 0.143\times\phi(^3\Pi(2431)), \tag{5-4}$$

$$\psi_{0+(III)} \approx 0.967\times\phi(^3\Pi(2341)) + 0.227\times\phi(^3\Sigma^-(2422)), \tag{5-5}$$

$$\psi_{0+(IV)} \approx 0.875\times\phi(^3\Sigma^-(2422)) + 0.445\times\phi(^1\Sigma^+(2422)). \tag{5-6}$$

Here, the spin-free state $^{2S+1}\Lambda$ with dominant configuration ($\sigma^p\pi^q\pi^{*r}\sigma^{*s}$) is denoted as $^{2S+1}\Lambda$ (*pqrs*). These valence orbitals of σ, π, π*, σ* denote the SA-SCF orbitals. Since the dipole moment operator is a spin-free operator, the transition dipole moment to the 0^+(III) state has a contribution from the largest component $^3\Pi(2341)$ of the state itself as shown in equation (5-7), while the one to the 0^+(IV) state has a contribution from the largest component $^1\Sigma^+(2440)$ of the ground state $X(0^+)$ as in equation (5-8),

$$\left\langle\psi_{X(0+)}\left|\hat{\mu}_z\right|\psi_{0+(III)}\right\rangle \approx 0.138\times\left\langle\phi(^3\Pi(2431))\left|\hat{\mu}_z\right|\phi(^3\Pi(2341))\right\rangle, \tag{5-7}$$

$$\left\langle\psi_{X(0+)}\left|\hat{\mu}_z\right|\psi_{0+(IV)}\right\rangle \approx 0.440\times\left\langle\phi(^1\Sigma^+(2440))\left|\hat{\mu}_z\right|\phi(^1\Sigma^+(2422))\right\rangle. \tag{5-8}$$

Since an excitation from the spin-free state $^1\Sigma^+(2440)$ to the state $^1\Sigma^+(2422)$ is approximately a two-electron process, the magnitude of the transition dipole moment between these states is 0.095 bohr, which is about one tenth of 0.90 bohr, the transition

dipole moment value between $^3\Pi(2431)$ and $^3\Pi(2341)$. The comparable magnitude of the transition dipole moments to the 0^+(III) and 0^+(IV) states is a consequence of the strong intensity borrowing of the 0^+(IV) state from the $^1\Sigma^+(2422)$ state and the large magnitude of the transition dipole moment between the spin-free states $^3\Pi(2431)$ and $^3\Pi(2341)$. The CI wave functions of this study yielded $\mu^2_{0+(\mathrm{III})} = 0.0172\ \mathrm{bohr}^2$ and $\mu^2_{0+(\mathrm{IV})} = 0.0091\ \mathrm{bohr}^2$, which are similar to the old values [42] of $\mu^2_{0+(\mathrm{III})} = 0.0179\ \mathrm{bohr}^2$ and $\mu^2_{0+(\mathrm{IV})} = 0.0099\ \mathrm{bohr}^2$.

With AO-like orbitals, the dominant configurations of the 0^+(III) state in the Franck-Condon region are $^3\Pi(2341)$ and $^3\Pi(1432)$. Those for the 0^+(IV) state are $^3\Sigma^-$(2422), $^3\Sigma^-(2332)$, and $^1\Sigma^+(2332)$. The interchange of these CSFs is clearly found at the avoided crossing Av-1 (Figure 5-3), which suggests that non-adiabatic transition is of the Landau-Zener type. In this calculation, the phases of the electronic wave functions were fixed, so that the transition dipole moments from the ground state X(0^+) to both of the 0^+(III) and 0^+(IV) states become positive in the Franck-Condon region. It will be essential in later discussion that the theoretical NACT between the 0^+(III) and 0^+(IV) states $g_{\mathrm{III,IV}} = \langle \psi_{\mathrm{III}} | \partial / \partial R | \psi_{\mathrm{IV}} \rangle$ resulted in a positive value at the avoided crossing Av-1.

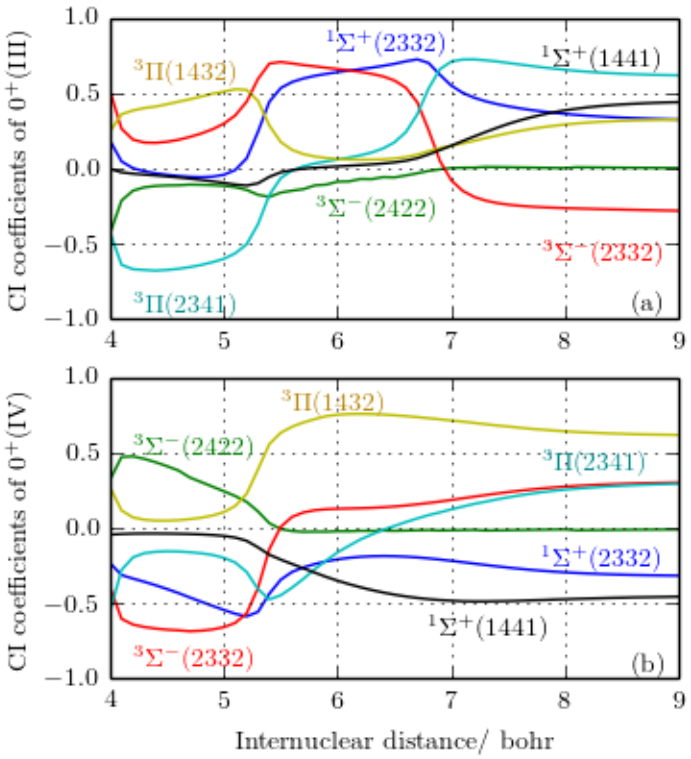

Figure 5-3: CI coefficients of (a) the 0^+(III) state and (b) the 0^+(IV) state in AO-like basis. Black curves are for $^1\Sigma^+$(1441). Blue curves are for $^1\Sigma^+$(2332). Red curves are for $^3\Sigma^-$(2332). Green curves are for $^3\Sigma^-$(2422). Light blue curves are for $^3\Pi$(2341). Yellow curves are for $^3\Pi$(1432). The numbers in parentheses represent the electronic configuration in AO-like basis.

5.3.2 Numerical calculation of the branching ratios and the anisotropy parameters

Using the classical path method, R is treated classically, and the time-dependent electronic wave function $\psi(t)$ can be expressed in the form of an expansion of the adiabatic basis $\psi_{\mathrm{III,IV}}(R)$, which evolves in time t, as [9,89]

$$\psi(t) = c_{\mathrm{III}}(t)\psi_{\mathrm{III}}(R(t))\exp[-\frac{i}{\hbar}\int_0^t E_{\mathrm{III}}(R(t'))\mathrm{d}t'] + c_{\mathrm{IV}}(t)\psi_{\mathrm{IV}}(R(t))\exp[-\frac{i}{\hbar}\int_0^t E_{\mathrm{IV}}(R(t'))\mathrm{d}t']. \quad (5\text{-}9)$$

Substituting Ψ into electronic time-dependent Schrödinger equation leads to

$$\dot{c}_{\mathrm{III}} = -\dot{R}(t)g_{\mathrm{III,IV}}(R(t))\exp[-\frac{i}{\hbar}\int_0^t (E_{\mathrm{IV}}(R(t')) - E_{\mathrm{III}}(R(t')))\mathrm{d}t']c_{\mathrm{IV}}, \quad (5\text{-}10)$$

$$\dot{c}_{\mathrm{IV}} = -\dot{R}(t)g_{\mathrm{IV,III}}(R(t))\exp[-\frac{i}{\hbar}\int_0^t (E_{\mathrm{III}}(R(t')) - E_{\mathrm{IV}}(R(t')))\mathrm{d}t']c_{\mathrm{III}}. \quad (5\text{-}11)$$

Here, R is considered to satisfy the classical equation of motion with the classical Ehrenfest force expressed as $F = -\partial\langle H\rangle / \partial R$, where the averaged potential energy of the 0^+(III) and 0^+(IV) states is given as

$$\langle H\rangle = |\, c_{\mathrm{III}}(t)\,|^2\; E_{\mathrm{III}}(R(t)) + |\, c_{\mathrm{IV}}(t)\,|^2\; E_{\mathrm{IV}}(R(t)). \quad (5\text{-}12)$$

The initial value of the internuclear distance $R(t=0)$ is selected as the classical turning point, where the averaged potential energy defined above equals to the sum of each photon energy and the ground vibrational level of the X(0^+) state. There, the initial values of the coefficients c_{III} and c_{IV} are given by the normalized transition dipole moments, $\mu_{\mathrm{III}}/\sqrt{\mu_{\mathrm{III}}^2 + \mu_{\mathrm{IV}}^2}$ and $\mu_{\mathrm{IV}}/\sqrt{\mu_{\mathrm{III}}^2 + \mu_{\mathrm{IV}}^2}$, respectively, and the classical internuclear velocity equals to zero $\dot{R} = 0$.

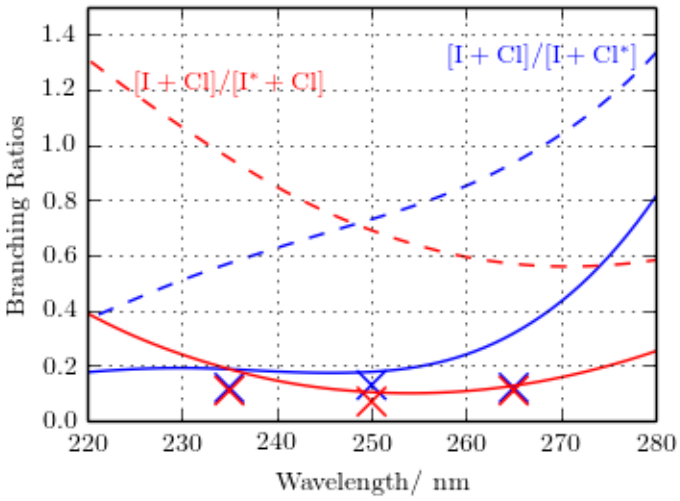

Figure 5-4: Branching ratios [I+Cl]/[I*+Cl] (blue) and [I+Cl]/[I+Cl*] (red). Solid curves are the calculations of classical path method with quantum interference effect. Dashed curves are the calculations without quantum interference effect. Cross markers represent the branching ratios observed by Diamantopoulou et al. [86].

Figure 5-4 for the calculated branching ratios [I+Cl]/[I*+Cl] and [I+Cl]/[I+Cl*] shows that large discrepancies existed previously are now resolved by including the quantum interference effect with which the present theoretical calculations are in good agreement with the experiment [86]. As Figure 5-5 shows, without quantum interference effect, the anisotropy parameter β for the I + Cl channel is dominated by the parallel component, in disagreement with experiment, especially on the longer wavelength side. However, with quantum interference effect, theoretical β for that channel exhibits a sharp decrease with an increasing wavelength, in general agreement with the experiment behavior. Figure 2-3 and Figure 5-2 show that, among three perpendicular states in the

second absorption band, only the 1(III) state correlates to the I + Cl product with a very weak absorption peak around 260 nm. Therefore, the results suggest that the sharp decrease in the experimental β parameter from 235 to 250 nm is caused by the switchover of the dominating components, from those originated from the 0^+(III) and 0^+(IV) states on the shorter wavelength side to those from the 1(III) state on the longer wavelength side. Because both of these components are very weak, the theoretical results of this study might slightly underestimate the perpendicular component at 250 and 265 nm.

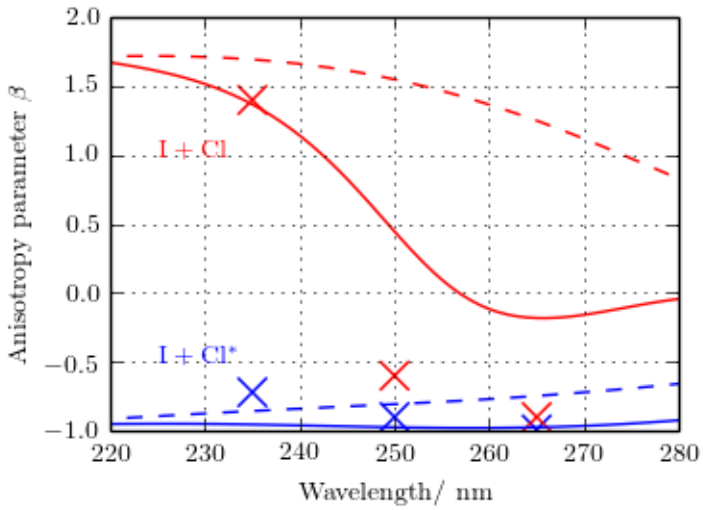

Figure 5-5: Anisotropy parameter β of the I+Cl* channel (blue) and the I+Cl channel (red). Solid curves are the calculation of the classical path method with quantum interference effect. Dashed curves are the calculations without quantum interference effect. Cross markers represent the anisotropy parameter β observed by Diamantopoulou et al. [86].

The norm of the 0^+(III,IV) states exhibits a drastic change at the avoided crossing Av-1 (Figure 5-6). It is essential that, while the parallel contribution of the I+Cl channel

was overestimated in previous numerical estimation [41,86], the quantum interference between the 0^+(III) and 0^+(IV) states included in the this calculation, contributes to the norm of the 0^+(III) state destructively, and to that of the 0^+(IV) state constructively.

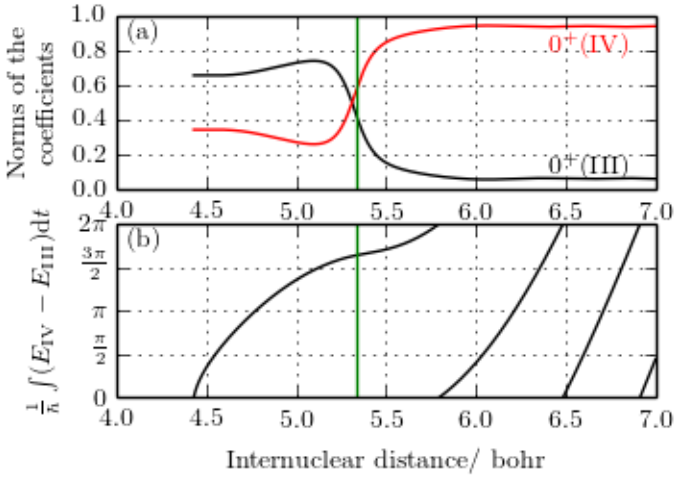

Figure 5-6: (a) Norms of the state amplitudes of the 0^+(III) and 0^+(IV) states and (b) phase difference between these states at 250 nm. Green vertical lines indicate the internuclear distance at Av-1.

5.3.3 Perturbation analysis of the non-adiabatic interaction

By treating the non-adiabatic interaction between the 0^+(III) and 0^+(IV) states as time-dependent perturbation, the first-order perturbation coefficient K_{III} of the adiabatic electronic 0^+(III) state in the asymptotic limit can be written as

$$
\begin{aligned}
K_{\mathrm{III}} &= \lim_{t\to\infty}\langle \psi_{\mathrm{III}}(R(t))|\psi(t)\rangle \\
&= \lim_{t\to\infty}\exp[-\frac{i}{\hbar}\int_0^t E_{\mathrm{III}}(R(t'))\mathrm{d}t']c_{\mathrm{III}}(t) \\
&= \exp[-\frac{i}{\hbar}\int_0^\infty E_{\mathrm{III}}(R(t))\mathrm{d}t]c_{\mathrm{III}}(0) \\
&-\int_0^\infty \dot{R}(t)g_{\mathrm{III,IV}}(R(t))\exp[-\frac{i}{\hbar}\int_0^t E_{\mathrm{IV}}(R(t'))\mathrm{d}t' - \frac{i}{\hbar}\int_t^\infty E_{\mathrm{III}}(R(t'))\mathrm{d}t']\mathrm{d}t c_{\mathrm{IV}}(0).
\end{aligned}
\tag{5-13}
$$

Following the treatment by Miller and George [89], the integration of the above second term can be evaluated with the stationary phase approximation, then expressed as a proportional constant A times the integrand at the time t_0 at which the above phase factor is the least varying, $(\mathrm{d}/\mathrm{d}t)(E_{\mathrm{IV}} - E_{\mathrm{III}}) = 0$, and also the magnitude of the integrand $\dot{R}g_{\mathrm{III,IV}}$ is the most dominant [89]. Since the NACT $g_{\mathrm{III,IV}}$ has a local maximum and the PECs of the 0^+(III,IV) states have the closest point at the avoided crossing Av-1, the two conditions of the stationary phase are satisfied when R is at Av-1. The above proportional constant A is positive and given by the asymptotic form of the Airy function as in equation (3.26) in [89]. Therefore, equation (5-13) is given as

$$
\begin{aligned}
K_{\mathrm{III}} &= \exp[-\frac{i}{\hbar}\int_0^\infty E_{\mathrm{III}}(R(t))\mathrm{d}t]c_{\mathrm{III}}(0) \\
&- A\dot{R}(t_0)g_{\mathrm{III,IV}}(R(t_0))\exp[-\frac{i}{\hbar}\int_0^{t_0} E_{\mathrm{IV}}(R(t))\mathrm{d}t - \frac{i}{\hbar}\int_{t_0}^\infty E_{\mathrm{III}}(R(t))\mathrm{d}t]c_{\mathrm{IV}}(0).
\end{aligned}
\tag{5-14}
$$

Similarly, the first-order perturbation coefficient K_{IV} of the electronic 0^+(IV) state in the asymptotic limit can be written as

$$K_{\mathrm{IV}} = \exp[-\frac{i}{\hbar}\int_0^{\infty} E_{\mathrm{IV}}(R(t))\mathrm{d}t]c_{\mathrm{IV}}(0) + A\dot{R}(t_0)g_{\mathrm{III,IV}}(R(t_0))\exp[-\frac{i}{\hbar}\int_0^{t_0} E_{\mathrm{III}}(R(t))\mathrm{d}t - \frac{i}{\hbar}\int_{t_0}^{\infty} E_{\mathrm{IV}}(R(t))\mathrm{d}t]c_{\mathrm{III}}(0). \quad (5\text{-}15)$$

It is safe to proceed without taking care of the normalization of these coefficients K_{III}, K_{IV}, since this formulation is intended to clarify the characteristics of the quantum interference in the 0^+(III,IV) states. Although the mixing of the two adiabatic states was not apparent from the coupled equations (5-9), (5-10), and (5-11), equations (5-14) and (5-15) clarify $K_{\mathrm{III,IV}}$ are expressed in terms of the superposition of the two adiabatic electronic states with the perturbative treatment. The norms of these K_{III}, K_{IV} for evaluating the branching rations give rise to not only the incoherent terms which have been evaluated in previous studies [86], but also the coherent term, which represents the quantum interference between the 0^+(III) and 0^+(IV) states, as

$$|K_{\mathrm{III}}|^2 = c_{\mathrm{III}}(0)^2 + A^2\dot{R}(t_0)^2 g_{\mathrm{III,IV}}(R(t_0))^2 c_{\mathrm{IV}}(0)^2 - A\dot{R}(t_0)g_{\mathrm{III,IV}}(R(t_0))c_{\mathrm{III}}(0)c_{\mathrm{IV}}(0)\cos[1/\hbar\int_0^{t_0}(E_{\mathrm{IV}} - E_{\mathrm{III}})\mathrm{d}t], \quad (5\text{-}16)$$

$$|K_{\mathrm{IV}}|^2 = c_{\mathrm{IV}}(0)^2 + A^2\dot{R}(t_0)^2 g_{\mathrm{III,IV}}(R(t_0))^2 c_{\mathrm{III}}(0)^2 + A\dot{R}(t_0)g_{\mathrm{III,IV}}(R(t_0))c_{\mathrm{III}}(0)c_{\mathrm{IV}}(0)\cos[1/\hbar\int_0^{t_0}(E_{\mathrm{IV}} - E_{\mathrm{III}})\mathrm{d}t]. \quad (5\text{-}17)$$

The repulsive potential energy curves of the 0^+(III,IV) states ensure that the velocity $\dot{R}$ is positive when passing the avoided crossing Av-1. The remaining coefficients $g_{\mathrm{III,IV}}(R(t_0))c_{\mathrm{III}}(0)c_{\mathrm{IV}}(0)$ are all positive, since the transition dipole moments to the 0^+(III,IV) states are both positive, and under the phase convention in this study, the resulting NACT between the 0^+(III) and 0^+(IV) states is positive at the avoided crossing

Av-1 (Figure 5-1). The common phase factor appearing in the coherent terms of equations (5-16) and (5-17) is calculated from the phase difference between the 0^+(III) and 0^+(IV) states at the avoided crossing Av-1 and is close to 2π, as Figure 5-6 shows. Hence, the quantum interference term for the 0^+(III) state shows destructive behavior, while the one for the 0^+(IV) state shows constructive behavior. Note that the integrand of the quantum interference term depends on the internuclear distance $R(t)$ and the initial internuclear distance $R(t=0)$ depends on the excitation energy, thus the phase difference between the 0^+(III) and 0^+(IV) states depends on the excitation energy.

The expressions of equations (5-16) and (5-17) indicate that the characteristics of the quantum interference terms are independent of the phase convention for the electronic wave functions. If the phase of the electronic wave function of the 0^+(III) state is reversed, the signs of the initial coefficient $c_{III}(t=0)$ and thus of the NACT $g_{III,IV}(R(t_0))$ are simultaneously reversed, but the overall sign in the interference term remains the same. In this way, the phases of the transition dipole moments and the NACTs must be calculated with full care, so that the continuity of the electronic wave function is kept consistent. Contrary to the previous suggestion [83], the comparable magnitudes of the theoretically predicted transition dipole moments to the 0^+(III,IV) states turn out to be essential, because if either transition dipole moment is negligible, the quantum interference effect would be negligible.

5.3.4 Semi-classical treatment

The nonadiabatic dynamics of the 0^+(III,IV) states were further investigated using analytical scattering matrix for Landau-Zener type potential [7,90]. The adiabatic representation of these electronic states 0^+(III,IV) is transformed to the diabatic representation $\varphi_{1,2}$ by transformation angle ϑ,

$$\begin{pmatrix} |\varphi_1\rangle \\ |\varphi_2\rangle \end{pmatrix} = \begin{pmatrix} \cos\vartheta & -\sin\vartheta \\ \sin\vartheta & \cos\vartheta \end{pmatrix} \begin{pmatrix} |0^+(\mathrm{IV})\rangle \\ |0^+(\mathrm{III})\rangle \end{pmatrix}. \tag{5-18}$$

By convention [2], the phases of these electronic states are fixed so as the transformation angle ϑ would be positive. The amplitudes at the turning point in adiabatic representation $X_{\pm}$ (in diabatic representation $X_{1,2}$) are connected to the amplitudes at the dissociation limit in adiabatic representation $A_{\pm}(+\infty)$ (in diabatic representation $A_{1,2}(+\infty)$) with reduced scattering matrix as follows [7,10,15],

$$\begin{pmatrix} A_-(+\infty) \\ A_+(+\infty) \end{pmatrix} = \begin{pmatrix} \exp(i\int k_- \mathrm{d}R) & 0 \\ 0 & \exp(i\int k_+ \mathrm{d}R) \end{pmatrix} \begin{pmatrix} \sqrt{1-e^{-2\pi\delta}}\, e^{-i\phi} & -e^{-\pi\delta} \\ e^{-\pi\delta} & \sqrt{1-e^{-2\pi\delta}}\, e^{i\phi} \end{pmatrix}$$
$$\times \begin{pmatrix} \exp(i\int k_- dR + \frac{i\pi}{4}) & 0 \\ 0 & \exp(i\int k_+ dR + \frac{i\pi}{4}) \end{pmatrix} \begin{pmatrix} X_- \\ X_+ \end{pmatrix}, \tag{5-19}$$

$$\begin{pmatrix} A_1(+\infty) \\ A_2(+\infty) \end{pmatrix} = \begin{pmatrix} \exp(i\int k_1 \mathrm{d}R) & 0 \\ 0 & \exp(i\int k_2 \mathrm{d}R) \end{pmatrix} \begin{pmatrix} e^{-\pi\delta} & -\sqrt{1-e^{-2\pi\delta}}\, e^{-i\phi} \\ \sqrt{1-e^{-2\pi\delta}}\, e^{i\phi} & e^{-\pi\delta} \end{pmatrix}$$
$$\times \begin{pmatrix} \exp(i\int k_1 dR + \frac{i\pi}{4}) & 0 \\ 0 & \exp(i\int k_2 dR + \frac{i\pi}{4}) \end{pmatrix} \begin{pmatrix} X_1 \\ X_2 \end{pmatrix}. \tag{5-20}$$

Here, subscripts +/ − represent the higher and lower adiabatic states, namely the 0^+(IV), 0^+(III) states, respectively, $k_\pm, k_{1,2}$ in the action integrals are the respective wavenumbers, defined as $\hbar k(R) = \sqrt{2\mu(E - V(R))}$, and the Stokes phase ϕ is analytically given as $\phi = \delta - \delta \ln \delta + \arg \Gamma(\delta) + \frac{\pi}{4}$, where the parameter δ is given in the reference [7,90]. The normalized transition dipole moments in the corresponding representation were used, as explained below equation (5-12), as the amplitudes at the turning point.

The branching ratio and the anisotropy parameter in the semi-classical method are shown in Figure 5-7 and Figure 5-8, respectively. Although they are in overall agreement with the experiment, there was a slight difference between the adiabatic and diabatic representations. In the adiabatic representation, the norms at the dissociation limit are given as,

$$|A_{III}|^2 = (1-p)X_{III}^2 + pX_{IV}^2 - 2X_{III}X_{IV}\sqrt{p(1-p)}\cos[\int_{R_{IV}}^{R_X} k_{IV}\mathrm{d}R - \int_{R_{III}}^{R_X} k_{III}\mathrm{d}R + \phi], \quad (5\text{-}21)$$

$$|A_{IV}|^2 = (1-p)X_{IV}^2 + pX_{III}^2 + 2X_{III}X_{IV}\sqrt{p(1-p)}\cos[\int_{R_{IV}}^{R_X} k_{IV}\mathrm{d}R - \int_{R_{III}}^{R_X} k_{III}\mathrm{d}R + \phi]. \quad (5\text{-}22)$$

The third terms in equations (5-21) and (5-22) describe the contributions of the quantum interference, where their phase parts consist of the action integral and the Stokes phase. Although the Stokes phases in the adiabatic and diabatic representations were consistent, the action integral part had a slight difference between the two representations (Figure 5-9). Hence, the difference of the adiabatic and diabatic representations is due to the difference between the adiabatic and diabatic potential energy curves. The author also notes that the semi-classical phase differences in equations (5-21) and (5-22) are approximately equal to 2π. Therefore the quantum interference term in equations (5-21) and (5-22) has the effects on the norm of the two states at its largest.

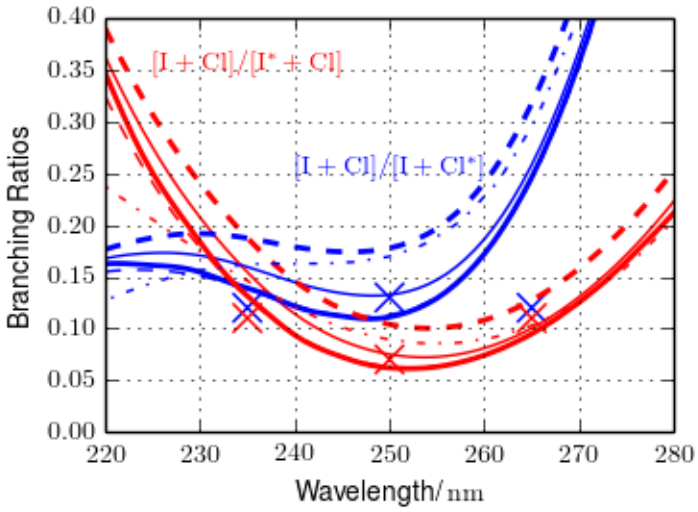

Figure 5-7: Branching Ratios [I+Cl]/[I*+Cl] (blue), [I+Cl]/[I+Cl*] (red). Dash-dot lines: Wave packet calculation with the interference effect. Thin solid lines: Semi-classical calculation in diabatic form. Thin

dashed lines: Semi-classical calculation in adiabatic form. Thick solid lines: Classical path method in diabatic form. Thick dashed lines: Classical path method in adiabatic form. Cross marker: Experiment by Diamantopoulou et al. [86]

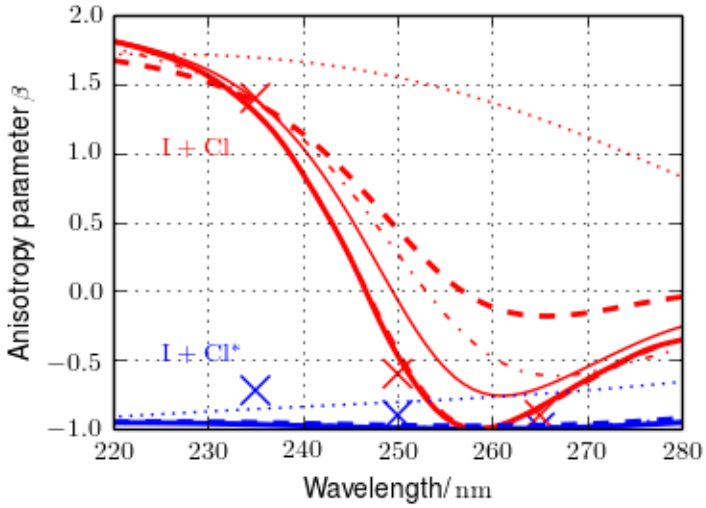

Figure 5-8: Anisotropy parameter β of the I+Cl* channel (blue) and the I+Cl channel (red). Dots: Wave packet calculation without the interference effect. Dash-dot lines: Wave packet calculation with the interference effect. Thin solid lines: Semi-classical calculation in diabatic form. Thin dashed lines: Semi-classical calculation in adiabatic form. Thick solid lines: Classical path method in diabatic form. Thick dashed lines: Classical path method in adiabatic form. Cross marker: Experiment by Diamantopoulou et al. [86].

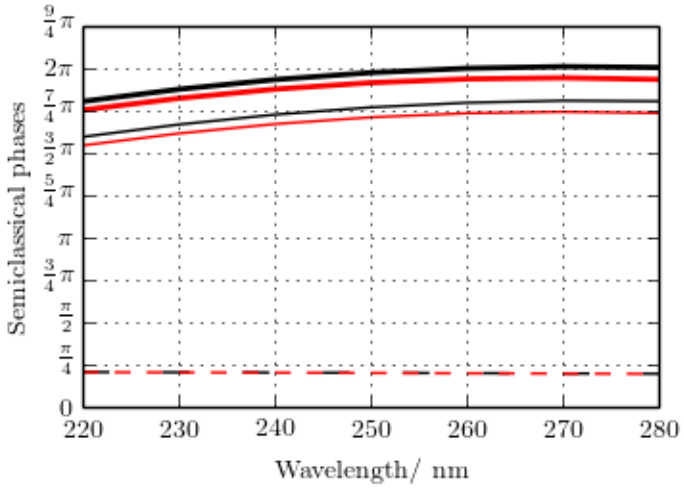

Figure 5-9: The semi-classical phases in adiabatic representation (black) and diabatic representation (red). Dashed lines: The Stokes phases ϕ. Thin lines: The phases of the action integral. Thick lines: The total phases.

5.4 Conclusions

The author studied the photodissociation process of ICl in the second absorption band. The branching ratios and the anisotropy parameters were calculated including the quantum interference effect between the 0^+(III) and 0^+(IV) states and the results are in better agreement with the experiments [83,86] than before. The comparable magnitudes of the transition dipole moments to the 0^+(III) and 0^+(IV) states are proved here to be important factors for the strong quantum interference effect. The weak excitation energy dependence of the quantum interference is one of the interesting features of this system. The author also discussed how the signs of the transition dipole moments and non-adiabatic coupling terms and the phase difference among the states affect the

characteristics of the quantum interference. Finally the author notes that the quantum interference effect may play an important role in a photodissociation process if the absorption spectra of the excited states overlap and non-adiabatic interactions among those states are non-negligible.

Chapter 6
General Conclusions

First, the theoretical transition dipole moments are essential information in the simulation of photodissociation process. Therefore, the author examined the theoretical transition dipole moment of Cl_2 molecule with various methods, to examine the accuracy. Although the calculation in the linear response treatment exhibited stability, the transition dipole moment in length form with MRSCI calculation showed better agreement with the experiment. Hence, the author employed the SASCF-MRSCI method for the transition dipole moment of ICl molecule.

Second, the product branching ratio, the anisotropy parameter β, and the first-rank angular momentum parameter $\mathrm{Im}[a_1^{(1)}(//,\perp)]$ in the first absorption band were calculated. For the product fraction and the β parameter, the author obtained the result supporting the experimental analysis by Samartzis and Kitsopoulos [66], and assigned that the obscure state is the z(1) state. For the first-rank angular momentum parameter $\mathrm{Im}[a_1^{(1)}(//,\perp)]$, the theoretical results showed quantitative agreement with phase part of the experimental data by Rakitzis et al. [23]. The disagreement with the simulation of Alexander and Rakitzis [68] is likely to be associated with the lack of the Stokes phase in their semi-

classical calculation. The non-adiabatic transition between the X(0^+) and 0^+(II) states was found to be of an Landau-Zener type without apparent avoided crossing between the two potential energy curves. Hence, the information of the potential energies alone is insufficient for calculating the non-adiabatic transition probabilities.

Third, the branching ratios and the anisotropy parameters in the second absorption band were calculated including the quantum interference effect between the 0^+(III) and 0^+(IV) states and the results are in better agreement with the experiments than before. The comparable magnitudes of the transition dipole moments to the 0^+(III) and 0^+(IV) states are proved here to be an important factor for the strong quantum interference effect. The calculation demonstrated how the signs of the transition dipole moments and non-adiabatic coupling terms and the phase difference among the states affect the characteristics of the quantum interference. Finally the author notes that the quantum interference effect may play an important role in a photodissociation process if the absorption spectra of the excited states overlap and non-adiabatic interactions among those states are non-negligible.

Finally, the ab initio calculations have shown overall agreement with the experiments and it has been demonstrated that the accuracy of the calculations is sufficient for evaluating the matter wave phase of the photofragments. The molecular dynamics calculations have been carried out with various methods, namely, the quantum mechanical wavepacket method, the classical path method, and the semi-classical method.

Among the three methods, the classical path method and the semi-classical method are applicable to large systems. In this study, the author clarified the importance of the phase consistency of the electronic state calculation and the necessity of calculating the non-adiabatic coupling terms for investigating the existence of avoided crossings. These findings hold for the molecular dynamics simulations not only for diatomic systems, but also for large systems. The quantum interference effects, which were studied in this thesis, are expected to play significant role in the molecular dynamics calculations of large systems.

References

[1] M. Born, R. Oppenheimer, Ann. Phys. 389 (1927) 457.

[2] F.T. Smith, Phys. Rev. 179 (1969) 111.

[3] P.A.M. Dirac, The Principles of Quantum Mechanics, Oxford University Press, Oxford, 1981.

[4] R.N. Zare, D.R. Herschbach, Proc. IEEE 51 (1963) 173.

[5] G.G. Balint-Kurti, R.N. Dixon, C.C. Marston, J. Chem. Soc. Faraday Trans. 86 (1990) 1741.

[6] G.G. Balint-kurti, M. Shapiro, Chem. Phys. 61 (1981) 137.

[7] S. Child, Molecular Collision Theory, Dover, Mineola, 1974.

[8] R.N. Zare, Mol. Photochem. 4 (1972) 1.

[9] E.E. Nikitin, Theory of Elementary Atomic and Molecular Processes in Gases, Clarendon Press, Oxford, 1974.

[10] H. Nakamura, Nonadiabatic Transition: Concepts, Basic Theories and Applications, World Scientific, Singapore, 2012.

[11] H. Lefebvre-Brion, R.W. Field, Perturbations in the Spectra of Diatomic Molecules, Academic Press, New York, 1986.

[12] L.D. Landau, Phys Z Sowjetunion 1 (1932) 285.

[13] C. Zener, Proc. R. Soc. Lond. Ser. A 137 (1932) 696.

[14] E.C.G. Stückelberg, Helv Phys ActaBasel 5 (1932) 369.

[15] M.S. Child, Semiclassical Methods in Molecular Scattering and Spectroscopy, Springer, New York, 1980.

[16] M.S. Child, R.B. Bernstein, J. Chem. Phys. 59 (1973) 5916.

[17] D.V. Kupriyanov, O.S. Vasyutinskii, Chem. Phys. 171 (1993) 25.

[18] M.H. Alexander, B. Pouilly, T. Duhoo, J. Chem. Phys. 99 (1993) 1752.

[19] T.P. Rakitzis, S.A. Kandel, R.N. Zare, J. Chem. Phys. 107 (1997) 9382.

[20] T.P. Rakitzis, S.A. Kandel, T. Lev-On, R.N. Zare, J. Chem. Phys. 107 (1997) 9392.

[21] T.P. Rakitzis, S.A. Kandel, A.J. Alexander, Z.H. Kim, R.N. Zare, Science 281 (1998) 1346.

[22] A.S. Bracker, E.R. Wouters, A.G. Suits, O.S. Vasyutinskii, J. Chem. Phys. 110 (1999) 6749.

[23] T.P. Rakitzis, S.A. Kandel, A.J. Alexander, Z.H. Kim, R.N. Zare, J. Chem. Phys. 110 (1999) 3351.

[24] A.J. Alexander, R.N. Zare, Acc. Chem. Res. 33 (2000) 199.

[25] A.J. Alexander, Z.H. Kim, S.A. Kandel, R.N. Zare, T.P. Rakitzis, Y. Asano, S. Yabushita, J. Chem. Phys. 113 (2000) 9022.

[26] K.O. Korovin, B.V. Picheyev, O.S. Vasyutinskii, H. Valipour, D. Zimmermann, J. Chem. Phys. 112 (2000) 2059.

[27] T.P. Rakitzis, P.C. Samartzis, R.L. Toomes, T.N. Kitsopoulos, A. Brown, G.G. Balint-Kurti, O.S. Vasyutinskii, J.A. Beswick, Science 300 (2003) 1936.

[28] A.J. Alexander, J. Chem. Phys. 118 (2003) 6234.

[29] M.N.R. Ashfold, N.H. Nahler, A.J. Orr-Ewing, O.P.J. Vieuxmaire, R.L. Toomes, T.N. Kitsopoulos, I.A. Garcia, D.A. Chestakov, S.-M. Wu, D.H. Parker, Phys. Chem. Chem. Phys. 8 (2006) 26.

[30] M.L. Costen, G.E. Hall, Phys. Chem. Chem. Phys. 9 (2006) 272.

[31] U. Fano, Rev. Mod. Phys. 29 (1957) 74.

[32] W. Happer, Rev. Mod. Phys. 44 (1972) 169.

[33] R.N. Dixon, J. Chem. Phys. 85 (1986) 1866.

[34] G.E. Hall, P.L. Houston, Annu. Rev. Phys. Chem. 40 (1989) 375.

[35] A.J. Orr-Ewing, R.N. Zare, Annu. Rev. Phys. Chem. 45 (1994) 315.

[36] L.D.A. Siebbeles, M. Glass-Maujean, O.S. Vasyutinskii, J.A. Beswick, O. Roncero, J. Chem. Phys. 100 (1994) 3610.

[37] T.P. Rakitzis, R.N. Zare, J. Chem. Phys. 110 (1999) 3341.

[38] Y. Mo, T. Suzuki, J. Chem. Phys. 112 (2000) 3463.

[39] A.G. Suits, O.S. Vasyutinskii, Chem. Rev. 108 (2008) 3706.

[40] D.J. Seery, D. Britton, J. Phys. Chem. 68 (1964) 2263.

[41] K. Tonokura, Y. Matsumi, M. Kawasaki, H.L. Kim, S. Yabushita, S. Fujimura, K. Saito, J. Chem. Phys. 99 (1993) 3461.

[42] S. Yabushita, J. Mol. Struct. THEOCHEM 461–462 (1999) 523.

[43] P.W. Langhoff, S.T. Epstein, M. Karplus, Rev. Mod. Phys. 44 (1972) 602.

[44] K. Sasagane, F. Aiga, R. Itoh, J. Chem. Phys. 99 (1993) 3738.

[45] O. Christiansen, P. Jørgensen, C. Hättig, Int. J. Quantum Chem. 68 (1998) 1.

[46] E.F. Hayes, R.G. Parr, J. Chem. Phys. 43 (1965) 1831.

[47] P.G. Szalay, R.J. Bartlett, J. Chem. Phys. 103 (1995) 3600.

[48] R. Ahlrichs, P. Scharf, C. Ehrhardt, J. Chem. Phys. 82 (1985) 890.

[49] R.J. Gdanitz, R. Ahlrichs, Chem. Phys. Lett. 143 (1988) 413.

[50] P.G. Szalay, R.J. Bartlett, Chem. Phys. Lett. 214 (1993) 481.

[51] R. Ahlrichs, Comput. Phys. Commun. 17 (1979) 31.

[52] R. Ahlrichs, P. Scharf, in:, K.P. Lawley (Ed.), Adv. Chem. Phys., John Wiley & Sons, Inc., Hoboken, 2007, pp. 501–537.

[53] R.J. Bartlett, Recent Advances in Coupled-Cluster Methods, World Scientific, Singapore, 1997.

[54] R.N. Zare, Angular Momentum: Understanding Spatial Aspects in Chemistry and Physics, John Wiley & Sons, Inc., Hoboken, 1988.

[55] G. Breit, H.A. Bethe, Phys. Rev. 93 (1954) 888.

[56] M. Abramowitz, I.A. Stegun, Handbook of Mathematical Functions: With Formulas, Graphs, and Mathematical Tables, Dover, London, 1965.

[57] V.V. Kuznetsov, O.S. Vasyutinskii, J. Chem. Phys. 123 (2005) 034307.

[58] E.T. Whittaker, G.N. Watson, A Course of Modern Analysis: An Introduction to the General Theory of Infinite Processes and of Analytic Functions; with an Account of the Principal Transcendental Functions, Cambridge University Press, Cambridge, 1963.

[59] H. Nakamura, Int. Rev. Phys. Chem. 10 (1991) 123.

[60] H. Nakamura, J. Phys. Soc. Jpn. 41 (1986) 413.

[61] K. Raghavachari, J.A. Pople, Int. J. Quantum Chem. 20 (1981) 1067.

[62] P.-O. Nerbrant, B. Roos, A.J. Sadlej, Int. J. Quantum Chem. 15 (1979) 135.

[63] G.H.F. Diercksen, B.O. Roos, A.J. Sadlej, Chem. Phys. 59 (1981) 29.

[64] H. Lischka, R. Shepard, R.M. Pitzer, I. Shavitt, M. Dallos, T. Müller, P.G. Szalay, M. Seth, G.S. Kedziora, S. Yabushita, Z. Zhang, Phys. Chem. Chem. Phys. 3 (2001) 664.

[65] R.F. Barrow, D.A. Long, D.J. Millen, J.A. Coxon, in:, Mol. Spectrosc., The Chemical Society, London, 1972.

[66] P.C. Samartzis, T.N. Kitsopoulos, J. Chem. Phys. 133 (2010) 014301.

[67] M.S. de Vries, N.J.A. van Veen, M. Hutchinson, A.E. de Vries, Chem. Phys. 51 (1980) 159.

[68] A.J. Alexander, T.P. Rakitzis, Mol. Phys. 103 (2005) 1665.

[69] S. Ohnishi, Theoretical Study on the Non-Adiabatic Photodissociation Processes of ICl, Master's Thesis, Keio University, 2007.

[70] L. Fernandez Pacios, P.A. Christiansen, J. Chem. Phys. 82 (1985) 2664.

[71] L.A. LaJohn, P.A. Christiansen, R.B. Ross, T. Atashroo, W.C. Ermler, J. Chem. Phys. 87 (1987) 2812.

[72] K.A. Peterson, D. Figgen, E. Goll, H. Stoll, M. Dolg, J. Chem. Phys. 119 (2003) 11113.

[73] D.E. Woon, T.H. Dunning, J. Chem. Phys. 98 (1993) 1358.

[74] A. Pardo, J.J. Camacho, J.M.L. Poyato, J. Chem. Soc. Faraday Trans. 87 (1991) 2529.

[75] R. McWeeny, Methods of Molecular Quantum Mechanics, Academic Press, New York, 1989.

[76] S. Yabushita, Z. Zhang, R.M. Pitzer, J. Phys. Chem. A 103 (1999) 5791.

[77] D. Kosloff, R. Kosloff, J. Comput. Phys. 52 (1983) 35.

[78] H. Tal-Ezer, R. Kosloff, J. Chem. Phys. 81 (1984) 3967.

[79] R. Kosloff, J. Phys. Chem. 92 (1988) 2087.

[80] G.G. Balint-Kurti, A.J. Orr-Ewing, J.A. Beswick, A. Brown, O.S. Vasyutinskii, J. Chem. Phys. 116 (2002) 10760.

[81] R.D. Gordon, K.K. Innes, J. Chem. Phys. 71 (1979) 2824.

[82] M. Siese, F. Bässmann, E. Tiemann, Chem. Phys. 99 (1985) 467.

[83] L.J. Rogers, M.N.R. Ashfold, Y. Matsumi, M. Kawasaki, B.J. Whitaker, Chem. Phys. Lett. 258 (1996) 159.

[84] K.-W. Jung, T.S. Ahmadi, M.A. El-Sayed, J. Phys. Chem. A 101 (1997) 6562.

[85] M. Cheng, Z. Yu, X. Xu, D. Yu, Y. Du, Q. Zhu, Sci. China Chem. 55 (2012) 1148.

[86] N. Diamantopoulou, A. Kartakoulis, P. Glodic, T.N. Kitsopoulos, P.C. Samartzis, J. Chem. Phys. 134 (2011) 194314.

[87] S. Yabushita, K. Morokuma, Chem. Phys. Lett. 175 (1990) 518.

[88] W. England, L.S. Salmon, K. Ruedenberg, in:, Mol. Orbitals, Springer Berlin Heidelberg, Berlin, 1971, pp. 31–123.

[89] W.H. Miller, T.F. George, J. Chem. Phys. 56 (1972) 5637.

[90] C. Zhu, H. Nakamura, J. Chem. Phys. 102 (1995) 7448.